PCCP

Accepted Manuscript

ROYAL SOCIETY OF CHEMISTRY

www.rsc.org/pccp

Cite this: DOI: 10.1039/c0xx00000x

www.rsc.org/xxxxxx

ARTICLE TYPE

A unified diabatic description for electron transfer reactions, isomerization reactions, proton transfer reactions, and aromaticity.

Jeffrey R. Reimers[ab]*, Laura K. McKemmish,[cd] Ross H. McKenzie,[e] and Noel S. Hush[df]

Received (in XXX, XXX) Xth XXXXXXXXX 20XX, Accepted Xth XXXXXXXXX 20XX

DOI: 10.1039/b000000x

While diabatic approaches are ubiquitous for the understanding of electron-transfer reactions and have been mooted as being of general relevance, alternate applications have not been able to unify the same wide range of observed spectroscopic and kinetic properties. The cause of this is identified as the fundamentally different orbital configurations involved: charge-transfer phenomena involve typically either 1 or 3 electrons in two orbitals whereas most reactions are typically closed shell. As a result, two vibrationally coupled electronic states depict charge-transfer scenarios whereas three coupled states arise for closed-shell reactions of non-degenerate molecules and seven states for the reactions implicated in the aromaticity of benzene. Previous diabatic treatments of closed-shell processes have considered only two arbitrarily chosen states as being critical, mapping these states to those for electron transfer. We show that such effective two-state diabatic models are feasible but involve renormalized electronic coupling and vibrational coupling parameters, with this renormalization being property dependent. With this caveat, diabatic models are shown to provide excellent descriptions of the spectroscopy and kinetics of the ammonia inversion reaction, proton transfer in $N_2H_7^+$, and aromaticity in benzene. This allows for the development of a single simple theory that can semi-quantitatively describe all of these chemical phenomena, as well as of course electron-transfer reactions. It forms a basis for understanding many technologically relevant aspects of chemical reactions, condensed-matter physics, chemical quantum entanglement, nanotechnology, and natural or artificial solar energy capture and conversion.

Introduction

In the early years of quantum mechanics, it was soon recognized that what we now know as coupled diabatic potential-energy surfaces provided simple and intuitive descriptions of chemical reaction processes. The advantage of this approach is that diabatic surfaces are typically easy to represent using simple forms such as harmonic potentials or Morse oscillators, as is the coupling between them. They however lead to very complex adiabatic potential-energy surfaces when the Born-Oppenheimer[1] approximation is applied to them. While the adiabatic surfaces more closely reflect actual experimental properties, the diabatic surfaces provide significant insight, describing the complex world of Chemistry in terms of simple, generic, underlying principles, connecting to chemical intuition.

The key defining property of a diabatic state is that its electronic character does not change as the nuclear co-ordinates are changed. In contrast the electronic character of adiabatic states change significantly as the nuclear co-ordinates undergo large changes, particularly those associated with chemical reactions. This is illustrated in Figure 1, taken from van Voorhis et al..[2] It depicts what happens when a gas-phase NaCl molecule dissociates: at the equilibrium bond length, the ground state of the molecule is predominantly ionic Na^+–Cl^- and there is a low-lying excited state that is predominantly covalent or radical, Na–Cl, produced by transfer of an electron to neutralize the two ions.[3] However, as the molecule stretches, the electronic characters of both the ground state and the excited state change smoothly, until at large distances the ground state takes on predominantly the radical form $Na^{\bullet}$–$Cl^{\bullet}$. This crossover occurs because as the distance increases the radical state becomes the one of lowest energy. The labels "Na^+–Cl^-" and "$Na^{\bullet}$–$Cl^{\bullet}$" refer to the chemically intuitive diabatic states whilst the Born-Oppenheimer ground-state and excited-state potential energy surfaces reflect different mixings of these forms at each nuclear geometry.

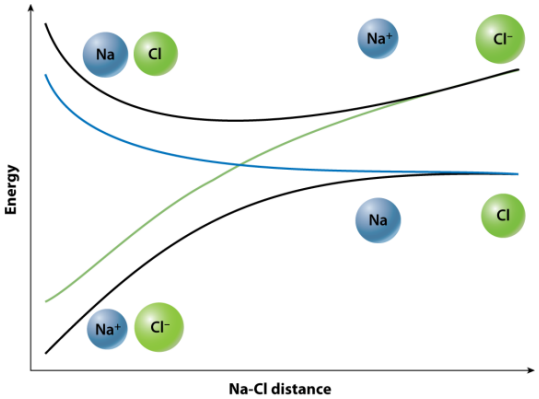

Fig. 1 Diabatic surfaces representing the Na^+–Cl^- (green) and $Na^{\bullet}$–$Cl^{\bullet}$ (blue) chemical descriptions of the NaCl molecule are mixed to give ground-state and excited-state adiabatic potential-energy surfaces (black). As the molecule stretches, the adiabatic surfaces change character whilst the diabatic surface do not. Taken from van Voorhis et al.,[2] reproduced with permission of *Annual Reviews*.

The impact of the diabatic-state picture is far reaching. In 1928 London interpreted[4] chemical reactions using what we now identify as a diabatic description. It was extended in 1931 by Eyring and Polanyi to construct the LEP adiabatic potential-energy surface[5] for general triatomic molecules.[6] In 1935 Horiuti and Polanyi[7] used this to introduce a coupled diabatic-surface description of proton transfer reactions, and these ideas were then applied to the ammonia inversion reaction by Wall and Glockler in 1937.[8] Hush later extended this to more general chemical processes in 1953.[9] However, London in 1932 also introduced a diabatic description of non-adiabatic processes[10] such as electron transfer that was more general than the perturbative treatments developed for reactions by Landau in the same year.[11, 12]

Today diabatic models provide the standard description of many chemical processes and their symmetry[13-19] especially electron-transfer[20-23] as this forms a basic model system.[2] Applications include: natural photosynthesis and organic photovoltaics,[24-35] chemical quantum computing,[36, 37] racemization processes,[38, 39] nonadiabatic photochemical reactions,[18, 19, 40-48] fluorescent methine dyes,[49] singlet exciton fission,[50] general double-bond isomerization processes,[51] and proton-transfer, hydrogen bonding, hydrogen-transfer, and coupled electron-proton transfer reactions.[52-62] Recently, we have shown that quite general adiabatic chemical reactions of the kind that are well represented using transition-state theory can also be quantitatively represented using diabatic functions,[63] demonstrating that the diabatic representation naturally gives rise to the revealing *reaction force* description of classic chemical reactions[64-66] and leads naturally to the Hammond-Leffler postulate[67, 68] concerning the nature of late and early transition states. Diabatic descriptions are also often essential within the generic *reaction path* description of chemical reactions,[69] are critical to spintronics,[70] and lead to basic understanding of the concept of aromaticity.[71-74] They are, however, not unique[2] and can be represented equivalently in many forms.[75]

Rather than starting with diabatic description of the ammonia inversion reaction,[17] the shapes of the ground-state double-well potentials in XY_3 molecules are conveniently described using valence-bond electron-pair repulsion theory[76-79] (VSEPR) and its origins.[80, 81] This approach focuses on the energetic benefit obtained when the geometry relaxes to minimize the electrostatic repulsion between electron pairs on the central atom X. An alternate simple approach is the applications of Walsh's Rules,[82-89] which focus on how the energies of the *occupied* orbitals change with molecular shape and electronegativity differences. Walsh's rules also allow for the prediction of excited-state properties, the analysis of which has been instrumental in the development of basic chemical understanding.[83, 90] However, classical thinking views the predictions made by the Walsh rules for ground and excited states as being *independent* whereas Bersuker[91-93] has stressed, using diabatic analyses, that it is also possible to view the ground-state properties as arising as a *manifestation* of the interactions between itself and a certain key excited state through the pseudo Jahn-Teller,[19, 94-96] Herzberg-Teller,[97] and related effects. This work stems from general theories of the symmetry of chemical reactions,[13-17] and the same critical concepts are captured in Shaik's "twin state" depiction of the properties of aromatic molecules.[71-74, 98]

More generally, understanding of the basic principle that ground-state properties and excited-state properties are intricately connected would have significant impact in unexpected areas such as the qualitative understanding of the successes and failures of Density-Functional Theory (DFT). It is widely appreciated that this is intrinsically a ground-state theory that is not optimized in any way to describe excited-state properties, yet the diabatic models tell us that the changes to the ground-state of a molecule as some property is varied (geometry, electric field, intermolecular interaction, interaction with radiation, etc.) depend critically on the properties of the excited states: if the excited states are improperly described then so are these ground-state properties. Hence the widely perceived view that excited-state properties should not be considered during the evaluation of density functionals is incorrect.

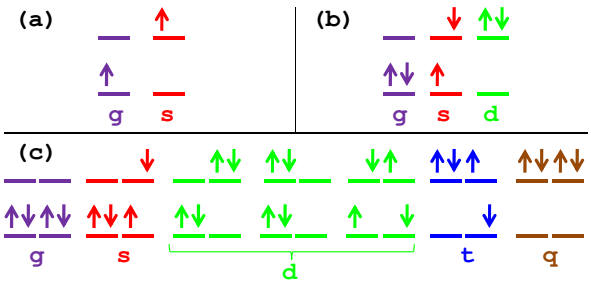

Fig. 2 Molecular-orbital diagrams showing representative unique electron occupations for the ground states *G*, singly excited states *S*, doubly excited states *D*, triply excited states *T* and quadruply excited states *Q*, where appropriate, for (a) electron transfer reactions involving radicals, (b) reactions between closed-shell species without orbital degeneracy, and (c) reactions between closed-shell species with doubly degenerate HOMO and LUMO orbitals. Note that only one spin component of each state is shown, as is one spatial component of the appropriate symmetry; the *G*, *D*, and *Q* states have one symmetry (totally symmetric for closed-shell reactions) whilst the *S* and *T* states have the opposite symmetry, the product of these symmetries being the symmetry of the coupling vibration.

However, only when applied to electron-transfer problems has diabatic theory previously been able to correlate *all* key ground-state and excited state properties of a system. Electron-transfer problems takes a particularly simple form as these processes are typically dominated by just two electronic states, as sketched e.g. in Fig. 2a. These states are simply identified as the "reactant" and "product" states and no other states are fundamentally required in the treatment, although it is not unusual to have close-lying states that interact and hence need to be included in expanded quantitatively accurate models.[51, 99] However, Fig. 2 also shows analogous scenarios in which the frontier orbitals involved in the process are closed shell, allowing more than one electron to contribute to the chemical process. These scenarios are seen to *inherently* generate more than two simultaneously coupled diabatic states. Always just the *two* of these states considered most critical have been kept in diabatic models, allowing most qualitative features of the chemistry to be adequately described.[19, 71-74, 98] However, the fitted parameters often have no apparent physical interpretation, can be very sensitive to small changes in the adiabatic surfaces,[63] and need different values to describe different properties. Considering explicitly only two states makes the assumption that a *single* conical-intersection seam controls the ground-state properties, but including all electrons and all coupled states indicates that, at the most fundamental level, *multiple* conical-intersection seams must be included.

In this paper, we construct simple diabatic models applicable to chemical processes for the closed-shell scenarios depicted in Fig. 2b and Fig. 2c. Fig. 2b depicts non-degenerate HOMO and LUMO frontier orbitals, as is applicable to e.g., hybridization, isomerization, hydrogen bonding, and many other reaction mechanisms, while Fig. 2c depicts doubly degenerate HOMO and LUMO orbitals, as found in benzene and is appropriate for the description of aromaticity. In the simplest complete diabatic description of these problems, all 3 electronic states shown in Fig.

2b must be included, and for Fig. 2c at least 5 of the 7.

However, we subsequently show that many properties of these systems can indeed be described adequately using effective two-state diabatic models, but that the parameters then become renormalized in ways that depend on the property of interest. Hence no universal set of two-diabatic-state parameters can describe all effects, explaining the lack of established semi-quantitative diabatic descriptions for general chemical reactions. Applied to benzene, it shows that Shaik's "twin state" concept[71-74] often used to motivate the nature of the benzene ground state is conceptually well founded but that the identity of the "twin state" has previously been misinterpreted- it is *not* the first excited electronic state as has been previously assumed. Nevertheless, the general multistate diabatic theory is both simple and semi-quantitatively accurate, allowing diabatic methods to be advanced as a simple way of describing chemical phenomena.

Section 2 reviews many mostly well-known critical results stemming from the application of two-state diabatic models to understand the adiabatic surfaces appropriate for symmetric electron-transfer reactions and spectroscopy,[100-104] using the properties of the iconic Creutz-Taube ion[105] $[(NH_3)_5Ru\text{-pyrazine-}Ru(NH_3)_5]^{5+}$ as an example. This section stresses how multiple ground-state and excited-state spectroscopic properties can be unified with structural and thermodynamic properties in a concise holistic chemical theory. Extracting the critical features of this analysis, Section 3 defines the concept of twinned states- a pair of states whose properties are intricately coupled, obeying the equations derived from electron-transfer theory. Section 4 derives the analogy between electron-transfer reactions and typical (non-degenerate) close-shell chemical reactions whilst Section 5 does this for benzene, considering the fundamental nature of aromaticity. These sections focus on the electronic states pertaining to general reactions that are twinned, obeying the laws of electron transfer theory once suitable renormalizations of the orbital properties are included.

As specific examples, hybridization and isomerization in ammonia, and proton transfer in $N_2H_7^+$, are discussed in Section 4. This analysis is kept to the most basic level, focusing on the essential features. In a companion paper, results from high-level ab initio calculations for the XH_3 and XH_3^+ series are processed using an expanded diabatic model that includes Rydberg states.[106] The critical result from this is that Rydberg states change the quantitative details in significant ways but not the underlying qualitative picture. However, interchange of the ordering of the Rydberg and valence orbitals from NH_3 to PH_3 is shown to provide the explanation of the very different bond angles observed in NH_3 (108°) and in PH_3, AsH_3, SbH_3, and BiH_3 (90-93°), an effect that VSEPR theory struggles to explain.[106] Also developed elsewhere are applications to understand the generic effects of the breakdown of the Born-Oppenheimer approximation,[107, 108] the development of quantum entanglement for use in quantum computing.[37] and detailed understanding of chemical reaction dynamics.[108]

2. Review and sample application of the basic 2-state diabatic coupling model

Here we present an overview of the critical results for symmetric reactions stemming from adiabatic electron-transfer theory,[75, 100-104, 109-114] using the Creutz-Taube ion $[(NH_3)_5Ru\text{-pyrazine-}Ru(NH_3)_5]^{5+}$ as an example. The potential-energy surfaces for this molecule obtained by fitting the observed[105, 115] intervalence absorption band using standard relationships[104] are shown in Fig. 3. The Creutz-Table ion is an important system as it was the first molecule discovered in which a single electron appeared to be

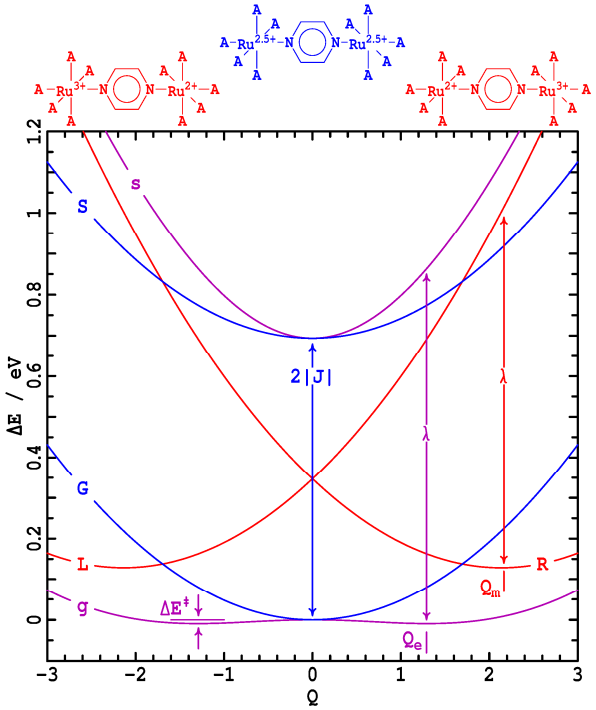

Fig. 3 Two-state potential-energy surfaces for the Creutz-Taube ion (A= NH_3) as a function of a (solvent-dominated) generalized dimensionless normal coordinate Q of a_u symmetry (J = 0.35 eV, λ =0.87 eV, Q_m =2.165 (ω/c =800 cm^{-1})): purple- ground and excited adiabatic states; red- localized diabatic representation as $(NH_3)_5Ru^{3+}$-pyrazine-$Ru^{2+}(NH_3)_5$ (L) and $(NH_3)_5Ru^{2+}$-pyrazine-$Ru^{3+}(NH_3)_5$ (R) diabatic potentials; blue- delocalized representation as ^2B_g (G) and ^2A_u (S) states of the diabatic potentials.

delocalized over two metallic sites, implying half-integral valence.[116, 117] Our current description of this ion indicates that it actually does have a double potential depicting integral metal valences but that this well is too shallow to support zero-point vibration.[116] This scenario leads to many observed properties that appear anomalous.[117] Shown in red in Fig. 3 are two diabatic potential-energy surfaces corresponding to charge-localized (unit-valence) structures of the form $(NH_3)_5Ru^{3+}$-pyrazine-$Ru^{2+}(NH_3)_5$ (L) and $(NH_3)_5Ru^{2+}$-pyrazine-$Ru^{3+}(NH_3)_5$ (R), structures that could be considered to be the "reactant" and "product" for an electron-transfer reaction. These species have different nuclear geometries located at minimum-energy values of $Q = \pm Q_m$ where $Q_m = 2.165$. Here, Q is a dimensionless normal coordinate representing the changes to the Ru-N bond lengths and other variables that occur when the charge transfers. These structures can be considered to be symmetrically related "isomers", and we represent them using purely harmonic potential-energy surfaces coupled by the resonance energy $|J|$ = 0.35 eV using the Hamiltonian matrix $\mathbf{H^{2L}}$ =

$$\begin{bmatrix} T + \frac{k}{2}(Q+Q_m)^2 + J - \frac{\lambda}{4} & J \\ J & T + \frac{k}{2}(Q-Q_m)^2 + J - \frac{\lambda}{4} \end{bmatrix} \quad (1)$$

expressed in terms of a diabatic electronic-state basis $\{\psi_L, \psi_R\}$. In this equation, $T = -\partial^2 / 2\mu'\partial Q^2$ is the nuclear kinetic energy operator, k is the effective force constant, μ' the effective mass,

the vibration frequency is $\omega = (k/\mu')^{1/2}$ =200 cm^{-1}, and

$$\lambda = 2kQ_m^2 = \frac{2\alpha^2}{k} = 2\alpha Q_m = 0.87 \text{ eV and } \alpha = Q_m / k \qquad (2)$$

are the reorganization energy (see Fig. 3) and vibronic coupling constant, respectively. The position variables Q and Q_m are expressed in terms of the vibrational zero-point length[118] $\sqrt{\hbar/\omega}$, identifying $k = \hbar\omega$ and $\mu' = 1/\hbar\omega$.

However, a simple unitary transformation[75] which rotates the basis-set vectors of Eqn. (1) by 45° allows this scenario to be equivalently represented as

$$\mathbf{H^{2D}} = \begin{bmatrix} T + \frac{k}{2}Q^2 & \alpha Q \\ \alpha Q & T + \frac{k}{2}Q^2 + 2J \end{bmatrix} \qquad (3)$$

in terms of delocalized diabatic electronic basis states $\{\psi_G, \psi_S\}$, where $\psi_G = [\psi_L - \psi_R]/2^{1/2}$ and $\psi_S = (\psi_L + \psi_R)/2^{1/2}$. This is the diabatic description most commonly used in spectroscopic analyses of high-symmetry molecules as the basis states now depict ground (G) and singly-excited (S) electronic states with minima at Q = 0 split in energy by $2J$ coupled by the vibronic couplings αQ. These surfaces are also shown in Fig. 3, in blue; this representation is the usual one applied say to discuss resonance and aromaticity in benzene, whilst in $\mathbf{H^{2L}}$ J manifests as the energy coupling term driving electron transfer.

The Born-Oppenheimer approximation is then introduced to produce the adiabatic potential-energy surfaces shown in magenta in Fig. 3 by parametric diagonalization of *either* Eqn. (1) or Eqn. (3) at each nuclear coordinate Q. The lower ground state surface (g) has a shallow double well while the upper surface (s) is single-welled. At the symmetric geometry Q = 0, these two adiabatic surfaces are separated in energy by 2|J|. Specifically, the adiabtaic surfaces are given by

$$\begin{aligned} \varepsilon_g(Q) &= \frac{k}{2}Q^2 + J - \left(J^2 + \alpha^2 Q^2\right)^{1/2} \\ &= \frac{\lambda}{4}\left(\frac{Q}{Q_m}\right)^2 + |J|\left\{1 - \left[1 + \left(\frac{\lambda}{2J}\right)^2\left(\frac{Q}{Q_m}\right)^2\right]^{1/2}\right\}, \\ \varepsilon_s(Q) &= \frac{k}{2}Q^2 + J + \left(J^2 + \alpha^2 Q^2\right)^{1/2} \\ &= \frac{\lambda}{4}\left(\frac{Q}{Q_m}\right)^2 + |J|\left\{1 + \left[1 + \left(\frac{\lambda}{2J}\right)^2\left(\frac{Q}{Q_m}\right)^2\right]^{1/2}\right\} \end{aligned} \qquad (4)$$

so that their difference is

$$\begin{aligned} \varepsilon_s(Q) - \varepsilon_g(Q) &= 2\left(J^2 + \alpha^2 Q^2\right)^{1/2} \\ &= 2|J|\left\{1 - \left[1 + \left(\frac{\lambda}{2J}\right)^2\left(\frac{Q}{Q_m}\right)^2\right]^{1/2}\right\}. \end{aligned} \qquad (5)$$

The ground-state and excited-state adiabatic vibration frequencies at the high-symmetry (Q=0) structure are then given by

$$\omega_i = \omega\left(1 - \frac{\lambda}{2|J|}\right)^{1/2} \qquad (6)$$

and

$$\omega_s = \omega\left(1 + \frac{\lambda}{2|J|}\right)^{1/2}, \qquad (7)$$

respectively.[119] Previous approaches at establishing analogies between electron-transfer theory and general chemical reactions have exploited this property, defining the excited state as the "twin state" of the ground state.[71-74] When $2|J|/\lambda < 1$, ω_i is imaginary[119] (i.e., ω_i^2 <0) and the adiabatic surface has a double-minimum with equilibrium geometries centered about $\pm Q_e$ where

$$\begin{aligned} Q_e &= Q_m\left[1 - \left(\frac{2J}{\lambda}\right)^2\right]^{1/2} \quad \text{i.e.,} \\ \left(\frac{2J}{\lambda}\right)^2 &= 1 - \left(\frac{Q_e}{Q_m}\right)^2. \end{aligned} \qquad (8)$$

The ground state vibration frequency then becomes

$$\omega_g = \omega\left[1 - \left(\frac{2J}{\lambda}\right)^2\right]^{1/2}, \qquad (9)$$

while the activation energy for reaction on the ground-state surface (see Fig. 3) is

$$\Delta E^{\ddagger} = \frac{\lambda}{4}\left(1 - \frac{2|J|}{\lambda}\right)^2 = \frac{|J|}{2}\frac{\lambda}{2|J|}\left(1 - \frac{2|J|}{\lambda}\right)^2 = \frac{(\lambda - 2|J|)^2}{4\lambda} \qquad (10)$$

Alternatively, if $2|J|/\lambda > 1$ then ω_i is real and depicts the ground-state vibration frequency; when $2|J|/\lambda = 1$, $\omega_g = \omega_i = 0$ and the ground-state potential is extremely anharmonic.

These equations lead to other useful relationships connecting the adiabatic properties that are independent of the diabatic frequency ω and hence the reduced mass including

$$\left(\frac{\omega_s}{\omega_i}\right)^2 = \frac{2|J| + \lambda}{2|J| - \lambda} \text{ or } \frac{2|J|}{\lambda} = \frac{\omega_s^2 + \omega_i^2}{\omega_s^2 - \omega_i^2} \qquad (11)$$

and, for double-well systems,

$$\begin{aligned} |J| &= 2\Delta E^{\ddagger}\frac{2|J|}{\lambda}\left(1 - \frac{2|J|}{\lambda}\right)^{-2} \\ &= \frac{\lambda}{2} - \sqrt{\lambda\Delta E^{\ddagger}}, \end{aligned} \qquad (12)$$

$$\begin{aligned} \lambda &= 4\Delta E^{\ddagger}\left(1 - \frac{2|J|}{\lambda}\right)^{-2} \\ &= 2\Delta E^{\ddagger} + 2|J| + 2\left[(\Delta E^{\ddagger})^2 + 2|J|\Delta E^{\ddagger}\right]^{1/2}, \end{aligned} \qquad (13)$$

$$\begin{aligned} \left(\frac{\omega_g}{\omega_i}\right)^2 &= -\frac{2|J|}{\lambda}\left(1 + \frac{2|J|}{\lambda}\right) \text{ or alternatively} \\ \frac{2|J|}{\lambda} &= -\frac{1}{2} + \left[\frac{1}{4} - \left(\frac{\omega_g}{\omega_i}\right)^2\right]^{1/2}, \end{aligned} \qquad (14)$$

and

$$\left(\frac{\omega_g}{\omega_s}\right)^2 = \frac{2|J|}{\lambda}\left(1 - \frac{2|J|}{\lambda}\right) \text{ or alternatively} \qquad (15)$$

$$\frac{2|J|}{\lambda} = \frac{1}{2} \pm \left[\frac{1}{4} - \left(\frac{\omega_g}{\omega_s} \right)^2 \right]^{1/2} .$$

Eqn. (15) indicates that $\omega_s \geq 2\omega_g$, equal for $2|J|/\lambda = 1/2$, with the counter-intuitive result $\omega_s / \omega_g \to \infty$ as $2|J|/\lambda \to 0$ or 1. It is well known that the excited-state harmonic frequency must exceed that of the ground state,[120] but here we see that it must at least *double* it when the ground-state is double welled, and can grow unbounded in *two* different ways.

When the ground-state diabatic surface is single welled, the adiabatic transition energy $h\nu$ measured by say UV/Vis spectroscopy is simply $2|J|$, but when it is double welled the energy is obtained by substituting Eqn. (8) into Eqn. (5) yielding simply λ. Another counter-intuitive result is thus that the energy gap λ between the diabatic potentials at the diabatic minimum-energy geometry is also the energy gap between the adiabatic potentials at the adiabatic minimum-energy geometry, see Fig. 3. Summarizing, we have:

$$\begin{aligned} h\nu = \varepsilon_s(Q_e) - \varepsilon_g(Q_e) &= 2|J| \quad \text{if } \frac{2|J|}{\lambda} \geq 1 \\ &= \lambda \quad \text{if } \frac{2|J|}{\lambda} \leq 1 \end{aligned} . \qquad (16)$$

This result for $2|J|/\lambda < 1$ is poorly known, it being common to use the approximation $h\nu \approx \varepsilon_s(Q_m) - \varepsilon_g(Q_m) = \left(4J^2 + \lambda^2\right)^{1/2}$.

Equations (12)-(16) present a variety of means through which the critical model parameters $|J|$ and λ can be determined from experimental or calculated data coming from ground-state or excited-state spectroscopy, the ground-state structure, or reaction rates, and it is the ability of the diabatic approach to unify these diverse properties that gives it its power.[104] Using the equations presented so far, the third free parameter in the model (equivalently α, Q_m, or ω) can be determined if either the ground-state double-well equilibrium geometry or well depth is known (Eqns. (8) or (10)), or else if one ω_g, ω_i, or ω_s is known through Eqns. (9), (6), and (7), respectively.

Many other means are also available for determining the model parameters from experimental data, particularly if the intervalence absorption and/or emission bands between the ground and singly excited states are available.[75, 104, 109, 110] The energies, intensity, and widths of these bands allow for the unique determination of $|J|$ and λ, with dipole-moment changes observed using Stark spectroscopy also being useful.[109, 121, 122] The effective displacement Q_m (in one or more modes) is readily determined from observed Franck-Condon factors if high resolution spectra are available. However, these electronic transitions are typically broad and unresolved, but nevertheless high-resolution infrared transitions for the ground state can usually be measured, with the vibronic coupling to the excited state often producing intense phase-phonon lines (for instance, the most intense transitions in the infrared spectrum of the bacteriochlorophyll special-pair radical cation produced following primary charge separation during photosynthesis are not observed in the spectrum of the neutral bacteriochlorophyll dimer or a single bacteriochlorophyll-monomer cation[123]). Intense Raman lines are also expected and can provide critical information.[124, 125] We do not explore generalizations of these and other methods within this paper, however.

The two-state diabatic model is also readily generalizable to describe asymmetric molecules. Asymmetry may result from chemical substitution, static and dynamic environment interactions, external electric fields (Stark effect), or may be intrinsic to some process. In the nonadiabatic ($2|J|/\lambda \ll 1$) limit, the activation energy is traditionally expressed[101, 112, 126] as the energy at which the diabatic states cross less the coupling $\Delta E^{\ddagger} \approx (\lambda + E_0)^2 / 4\lambda - |J|$. However improved expressions also encompassing Eqn. (13) valid if *either* $2|J|/\lambda$ *or* E_0/λ are small (i.e., away from the region in which the double-minimum disappears) are

$$\begin{aligned} \Delta E^{\ddagger} &\approx \frac{\lambda}{4}\left(1 + \frac{2E_0}{\lambda} - \frac{4|J|}{\lambda} + \frac{E_0^2}{\lambda^2} + \frac{4J^2}{\lambda^2} + \frac{2|J|E_0^2}{\lambda^3} \right) \\ &\approx \frac{\lambda}{4}\left(1 + \frac{E_0}{\lambda} - \frac{2|J|}{\lambda} \right)^2 \end{aligned} \qquad (17)$$

where E_0 is the (free) energy of reaction.[107] More general effects of asymmetry are also known,[75] including its effects on primary charge separation during photosynthesis[121] and on Stark spectroscopy.[110, 127] Herein we do not pursue these effects, but extension of the mathematics to do so is straightforward.[75]

A significant feature of the diabatic coupling model is the prediction of considerable anharmonicity for both the ground and excited state. While such anharmonicity is readily apparent and causes the appearance of the ground-state double-well for $2|J|/\lambda < 1$, it is equally large for the excited state in general as well as for the ground state when $2|J|/\lambda > 1$:

$$\frac{\partial^4 E_g}{\partial Q^4} = -\frac{\partial^4 E_s}{\partial Q^4} = \frac{3\alpha^4}{8|J|^3} . \qquad (18)$$

These strongly effect the ratios of the 0→1 vibrational transition energies in the ground and excited states, making Eqns. (12)-(15) difficult to apply to experimental data as $2J/\lambda \to 0$.

3. Twinned states

Electron-transfer theory naturally generates two diabatic states with a single conical-intersection seam, leading to the multitude of connected properties of the ground and excited states depicted by Eqns. (1)-(18). Following Shaik,[71-74, 98] we consider these two states to be *twinned*. Further, for general reactions not involving electron transfer, we define twinned state to be any pair for which the adiabatic energy levels can be described by an equation having the same form as Eqn. (4). The parameters in this equation may be renormalized, however, and understanding this process is critical to obtaining diabatic model parameters then can be compared for different chemical systems. Once the analogy to Eqn. (4) is established, Eqns. (1)-(18) then all hold, allowing many properties to be correlated. Table 1 captures the properties of twinned states for a variety of chemical systems, including the basic results for electron-transfer.

4. Three-state model for reactions between closed-shell species

As shown in Fig. 2b, not only do the ground diabatic state (*G*) and single excited diabatic state (*S*) arise for processes involving non-degenerate closed-shell orbitals but also a third double excited diabatic state (*D*). Simplistically, vibronic coupling

Cite this: DOI: 10.1039/c0xx00000x

www.rsc.org/xxxxxx

ARTICLE TYPE

Table 1. Parameter renormalization required for effective 2-state (twinned) models so that the adiabatic surfaces are given in the form of Eqn. (4) as $\varepsilon_{\pm}(Q) = kQ^2/2 + J' \mp (J'^2 + \alpha'^2 Q^2)^{1/2}$ (also defining $Q'_m = \alpha'/k, \lambda' = 2\alpha'^2/k$)

Problem	approximation	Twinned states		J'	α'	λ'	Q'_m	$2J'/\lambda'$
Electron/hole transfer: 1 electron/hole in 2 orbitals	none	g	s	J	α	λ	Q_m	$2J/\lambda$
Isomerization, hydrogen bonding, etc.: 2 electrons in 2 orbitals	none	g	d	$2J$	$2^{1/2}\alpha$	2λ	$2^{1/2}Q_m$	$2J/\lambda$
Aromaticity: 4 electrons in 4 orbitals	$Q^4 \ll 36(J/\alpha)^4$ [a]	g	q	$4J$	2α	4λ	$2Q_m$	$2J/\lambda$
Aromaticity: 4 electrons in 4 orbitals	$Q^4 \ll 36(J/\alpha)^4$ [a]	s	t	0	0	0	0	-
Aromaticity: 4 electrons in 4 orbitals	$Q^4 \gg 36(J/\alpha)^4$	g	q	$22^{1/2}J$	$3^{1/2}\alpha$	3λ	$3^{1/2}Q_m$	$(22/9)^{1/2}\,J/\lambda$
Aromaticity: 4 electrons in 4 orbitals	$Q^4 \gg 36(J/\alpha)^4$	s	t	$i2^{1/2}J$	α	λ	Q_m	$i2^{1/2}\,J/\lambda$

a: This applies to benzene at all normally accessable geometries, Q is substituted by the angle ϕ in text.

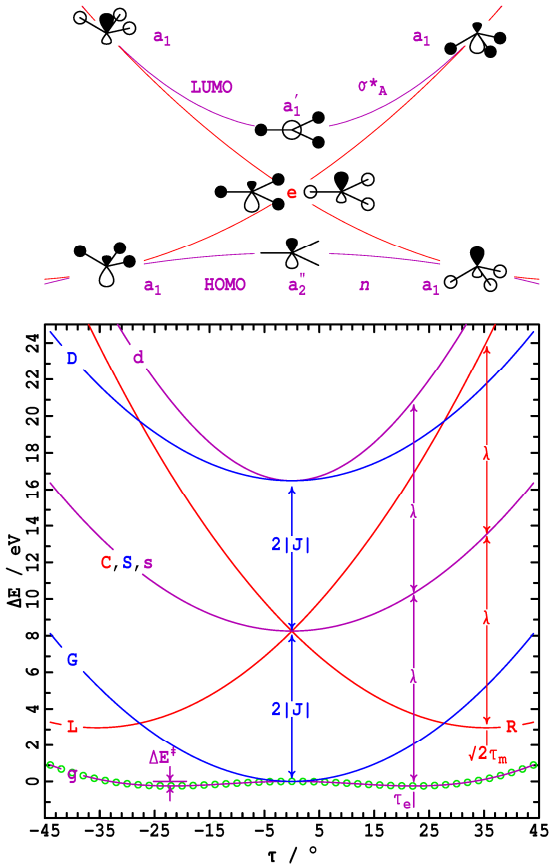

Fig. 4 The lower figure shows the Swalen and Ibers adiabatic potential for the torsional motion (ν_2 , a_2'') of NH_3 (green circles) fitted up to τ =44° (θ= 77°) by a 3-state 3-parameter diabatic-potential model ($|J|$ = 4.13 eV, λ =10.55 eV, δ =25.1°, RMS error 1.2 meV): purple- resulting adiabatic ground-state (G), singly valence-excited state (S), and doubly valence-excited state (D) (the "twin state"); red- localized representation of two of the diabatic potentials; blue- delocalized representation of the two of the diabatic potentials (both $^1A_1'$). The upper figure shows the adiabatic Walsh diagram for the HOMO (n, a_2'') and valence LUMO (σ^*_A, a_1') orbitals that generate these transitions (purple) and the associated (N sp hybrid mixed with H s) localized diabatic orbitals (red).

$$\mathbf{H^{3D}} = \begin{bmatrix} T + \frac{k}{2}Q^2 & \alpha Q & 0 \\ \alpha Q & T + \frac{k}{2}Q^2 + 2J & \alpha Q \\ 0 & \alpha Q & T + \frac{k}{2}Q^2 + 4J \end{bmatrix} \quad (19)$$

between S and D should parallel that between G and S as the same orbitals are involved. The indirect effect of D on G will therefore always be significant and cannot be neglected. In the delocalized diabatic representation, the simplest description possible for the interactions is therefore the Hamiltonian matrix expressed in terms of delocalized diabatic electronic basis states $\{\psi_G, \psi_S, \psi_D\}$. The three diabatic potential surfaces embodied in this equation are shown in blue in Fig. 4 for the case of the ammonia inversion reaction,[17, 83] where the general coordinate Q is replaced by the specific torsional angle τ.[118, 128] Also shown in this figure in red are three localized diabatic potential-energy surfaces obtained by rotating $\mathbf{H^{3D}}$ into the basis states $\{\psi_L, \psi_C, \psi_R\}$ using the rotation $\mathbf{H^{3L}} = \mathbf{R}^{\mathrm{T}}\mathbf{H^{3D}}\mathbf{R}$, where, defining $H_0 = T + 2J - \lambda/2$,

$$\mathbf{R} = \begin{bmatrix} \frac{1}{2} & \frac{1}{\sqrt{2}} & \frac{1}{2} \\ \frac{1}{\sqrt{2}} & 0 & \frac{-1}{\sqrt{2}} \\ \frac{-1}{2} & \frac{1}{\sqrt{2}} & \frac{-1}{2} \end{bmatrix} \quad (20)$$

and $\mathbf{H^{3L}} = H_0\mathbf{1} +$

$$\begin{bmatrix} \frac{k}{2}(Q + \sqrt{2}\,Q_m)^2 & -\sqrt{2}J & 0 \\ -\sqrt{2}J & \frac{k}{2}Q^2 + \frac{\lambda}{2} & \sqrt{2}J \\ 0 & \sqrt{2}J & \frac{k}{2}(Q - \sqrt{2}\,Q_m)^2 \end{bmatrix}. \quad (21)$$

Applying the Born-Oppenheimer approximation to either of these Hamiltonians, the corresponding adiabatic potential-energy surfaces (g), (s), and (d) are

$$\varepsilon_g = \frac{kQ^2}{2} + 2J - \left(4J^2 + 2\alpha^2 Q^2\right)^{1/2}$$
$$\varepsilon_s = \frac{kQ^2}{2} + 2J, \text{ and} \qquad (22)$$
$$\varepsilon_d = \frac{kQ^2}{2} + 2J + \left(4J^2 + 2\alpha^2 Q^2\right)^{1/2}$$

and these are shown in magenta in the Fig. 4. Most significantly, the couplings are seen to change the shape of only the *G* and *D* or *L* and *R* diabatic surfaces and not *S* or *C*. A simplistic interpretation is that the single excitation and central states behave as if they are *non-interacting*, with their adiabatic potentials exactly matching the diabatic ones, whilst an enhanced effective 2-state interaction akin to Eqn. (4) appears between *G* and *D* or *L* and *R*. It is possible to ignore the non-interacting states, generating effective two-state models whose properties parallel those identified for electron-transfer problems. The ground state *g* and the doubly excited state *d* are thus identified as being *twin states*.

Comparing these adiabatic surfaces in Eqn. (22) with those for the actual two-state model in Eqn. (4), a renormalization of the parameters is evident. This process is catalogued in Table 1. Equation (22) takes on the form of Eqn. (4), $\varepsilon_{\pm}(Q) = kQ^2/2 + J' \mp (J'^2 + \alpha'^2 Q^2)^{1/2}$, if the renormalization $J'=2J$, $\lambda'=2\lambda$, $\alpha'=2^{1/2}\alpha$, and $Q_m' = 2^{1/2} Q_m$ is used.

Applying a two-state model to interpret the properties of the *g* and/or *d* surfaces will return the renormalized properties *J'* and λ', while considering the properties of say a photochemical reaction from *s* to *g*, as is commonly done for charge-recombination reactions,[129] will yield the fundamental properties *J* and λ. Figure 4 stresses this, indicating that the easily observable spectroscopic transition energies at the equilibrium geometry of the ground adiabatic state, following Eqn. (16), are

$$\frac{2|J|}{\lambda} \geq 1: \quad h\nu_{gs} = \varepsilon_s(Q_e) - \varepsilon_g(Q_e) = 2|J| \;,\; h\nu_{ds} = 4|J|$$
$$\frac{2|J|}{\lambda} \leq 1: \quad h\nu_{gs} = \varepsilon_d(Q_e) - \varepsilon_g(Q_e) = \lambda \quad ,\; h\nu_{ds} = 2\lambda \qquad (23)$$

In summary, we see that different 2-state diabatic models are appropriate for different experiments, but the critical control ratio $2J'/\lambda' = 2J/\lambda$ is invariant (Table 1). However, another significant feature is that the basis states in which the effective two-state Hamiltonian is constructed are complex. Rotation matrices $\mathbf{H}^{\mathbf{3D\rightarrow 2D'}}$ and $\mathbf{H}^{\mathbf{3L\rightarrow 2L'}}$ can be identified that transform $\mathbf{H}^{\mathbf{3D}}$ and $\mathbf{H}^{\mathbf{3L}}$ into effective two-state Hamiltonians $\mathbf{H}^{\mathbf{2D'}}$ and $\mathbf{H}^{\mathbf{2L'}}$

$$\mathbf{H}^{\mathbf{2D'}} = \begin{bmatrix} T + \frac{k}{2}Q^2 & 0 & \sqrt{2}\alpha Q \\ 0 & T + \frac{k}{2}Q^2 + 2J & 0 \\ \sqrt{2}\alpha Q & 0 & T + \frac{k}{2}Q^2 + 4J \end{bmatrix} \qquad (24)$$

and $\mathbf{H}^{\mathbf{2L'}} = H_0\mathbf{1} +$

$$\begin{bmatrix} \frac{k}{2}(Q+\sqrt{2}Q_m)^2 & 0 & 2J \\ 0 & \frac{k}{2}Q^2 + \frac{\lambda}{2} & 0 \\ 2J & 0 & \frac{k}{2}(Q-\sqrt{2}Q_m)^2 \end{bmatrix}. \qquad (25)$$

These transformations are complex and are given in Electronic Supplementary Information (ESI). They are *not* diabatic transformations, however, as they are dependent on the nuclear coordinate *Q*, unlike say Eqn. (20). They preserve the adiabatic state energies but modify other properties such as transition moments and the entanglement between the vibrational and electronic degrees of freedom.[37, 108] Of particular significance is the nature of the transformation vectors that produce the non-interacting effective single-excitation adiabatic state. For the $\mathbf{H}^{\mathbf{3D\rightarrow 2D'}}$ transformation this vector is

$$\left[2 + \left(\frac{2J}{\alpha Q}\right)^2\right]^{-1/2} \begin{bmatrix} 1 \\ 2J/\alpha Q \\ 1 \end{bmatrix} \qquad (26)$$

so that the adiabatic single excitation state is made up mostly from the actual single excitation for $Q^2 \ll 2J^2/\alpha^2$ but is the valence-bond state comprised of an equal mixture of the ground-state and doubly-excited state for $Q^2 \gg 2J^2/\alpha^2$. The physical meaning of the pseudo-diabatic states used in effective 2-state models thus requires careful consideration.

$\mathbf{H}^{\mathbf{3L}}$ and $\mathbf{H}^{\mathbf{3D}}$ describe a 3-state 3-parameter diabatic model. However, for the interpretation of detailed calculated data for potential-energy surfaces, the assumption of identical vibronic coupling and energy gaps between the *G*, *S*, and *D* diabatic states does not provide for quantitative analysis. At least a 5-parameter model is required that allows these quantities to differ slightly, with *J* and α then being replaced with J_G, J_D and α_G, α_D for the *G*-*S* and *S*-*D* interactions, respectively. Also, intrinsic anharmonicities k_4 in the diabatic surfaces can become important, as well as third-order vibronic coupling contributions γ_G and γ_D, leading to an 8-parameter model. Finally, at the same level of approximation, three other parameters also arise, the second-order vibronic coupling connecting the ground-state with the doubly-excited state β, and possible changes to the force constants $\beta_G/2$ and $\beta_D/2$ owing to say interferences from nearby excited states, making in fact an 11-parameter model. The full equations pertaining to these situations are described in ESI, with in particular the revised Hamiltonians $\mathbf{H}^{\mathbf{3D}}$ and $\mathbf{H}^{\mathbf{3L}}$ defined in Eqns. (S5) and (S6), respectively. This leads to revised adiabatic vibration frequencies

$$\omega_i = \omega\left[1 - \frac{\lambda_G}{2|J_G|}\right]^{1/2},$$
$$\omega_s = \omega\left[1 + \frac{2\beta_G}{k} + \frac{\lambda_G}{2|J_G|} - \frac{\lambda_D}{2|J_D|}\right]^{1/2}, \text{ and} \qquad (27)$$
$$\omega_d = \omega\left[1 + \frac{2\beta_G + 2\beta_D}{k} + \frac{\lambda_D}{2|J_D|}\right]^{1/2}.$$

The anharmonicities of these surfaces can be described analytically (Eqn. S7), and from these expressions for the diabatic-model parameters obtained in terms of observable quantities (Eqn. S8).

In the simplistic situation with $J_D = J_G$ and $\lambda_D = \lambda_G$, ignoring other subtle effects by setting $\beta_G = \beta_D = \beta = 0$, these frequencies are ordered $\omega_i < \omega_s < \omega_d$. It is very unusual to have the excited-state frequency of a mode greater than its ground-state frequency as excitation usually breaks bonds and hence lowers frequencies. This unusual property is characteristic of strong

vibronic coupling.[120] If only the ground-state and singly-excited state are considered, i.e., only the states readily accessible by spectroscopic means, then it is natural to consider *s* as the "twin state" of *g*, thinking that these states are described by Eqns. (6) and (7), respectively. However, the doubly excited state has a higher frequency again and Eqns. (27) and (22) show that it is actually the twin state to the ground state.

Indeed, Eqn. (27) indicates that considering *s* as the twin state can easily lead to incorrect qualitative conclusions. It is possible that $2|J_G|/\lambda_G$ could differ significantly from $2|J_D|/\lambda_D$, significantly distorting the frequency of the singly excited state. In particular, it is possible that the ground-state is single-welled whilst the singly excited state is double welled if $2|J_G|/\lambda_G > 1$ and $\lambda_D/2|J_D| - \lambda_G/2|J_G| > 1$, a counter-intuitive result not anticipated by most discussions of "twin state" properties.

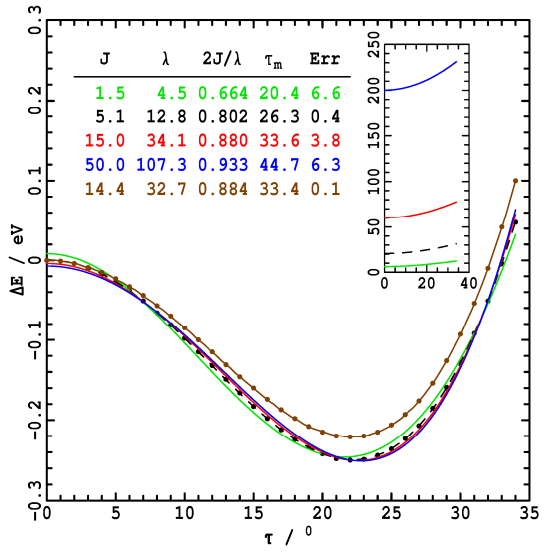

Fig. 5 The 1962 Swalen and Ibers[128] (black dots) and 2011 NH3-2010 Yurchenko et al.[130] (brown dots) adiabatic potentials *g* for the torsional motion (ν_2) of NH_3 are fitted up to 34° by various 3-state 3-parameter diabatic-potential models: black, brown dashed- all parameters optimized, else optimization with *J* constrained. The insert shows the associated double- excitation adiabatic surfaces whilst the tabulated diabatic potential parameters are *J* (eV), λ (eV) and τ_m (°), while the RMS error in the fits is also given (meV).

3a. Application to interpret experimentally derived potential-energy surfaces for the ammonia inversion reaction

The ammonia inversion reaction is a prototype for many chemical processes. In 1962 an analytical one-dimensional potential-energy function was fitted to observed spectroscopic data for the ground state of ammonia by Swalen and Ibers[128] and this is shown in Fig. 5. Using more sophisticated fitting techniques and vastly expanded experimental data, two multi-dimensional potential-energy surfaces were obtained in 2011 by Yurchenko et al.[130] and by Huang et al.[131], and the former, named NH3-Y2010, is also shown in the figure. These modern surfaces are very similar to the older one except that the well depth is reduced by 10% from 0.25 eV to 0.220 eV. Rather than using a dimensionless normal coordinate *Q*, this potential is plotted as a function of the improper torsional angle τ, with the diabatic and adiabatic minimum-energy geometries renamed from Q_m to τ_m and Q_e to τ_e, respectively. τ is defined as the angle between each NH bond and the plane containing the three H atoms;[118, 128] it is simply related to the HNH bond angle θ through

$$2\cos\theta = 3\sin^2\tau - 1 \qquad (28)$$

so that when $\tau = 0$, $\theta = 120°$, when $\theta = 90°$, $\tau = 35.26°$, and at the equilibrium geometry of the Swalan and Ibers / NH3-2010 potentials, $\tau_e = 22.2°$ / 22.0° and $\theta_e = 106.6°$ / 106.8°. The "effective mass" (really a moment of inertia) associated with this curvilinear torsional coordinate is dependent on the stretch coordinates,[128]

$$\mu = \frac{3mM + 9m^2\sin^2\tau}{M + 3m} r_{NH}^2 \qquad (29)$$

where *m* is the mass of H and *M* is the mass of N. Other choices of inversion coordinates are possible,[132] but use of a curvilinear coordinate in any simple model is essential.

For the Swalan and Ibers and NH3-2010 potentials, the equilibrium to barrier force-constant ratios can be expressed as $\omega_g/\omega_i = 1.220i$ and $1.295i$, respectively. Using the 3-parameter 3-state model (Eqn. (19) or (21)) in its effective 2-state form (Eqn. (24) or (25)), the analogous forms of Eqns. (8), (12), and (13) yield: $2J/\lambda = 0.82$ and 0.89, λ = 15.2 and 35.2 eV, *J* = 6.2 and 15.6 eV, and $\tau_m = 27.3°$ and 33.9°, giving α =0.28 and 0.52 eV/°^{2} (Eqn. (2)) and the force constant is *k* = 10.2 and 15.4 meV/°^{2} (Eqn. (2)). So while the two observed surfaces appear quite similar, they lead to very different values of the diabatic-model parameters. These different values arise as most equations become very sensitive as $2J/\lambda \to 1$, especially Eqns. (12) and (13) specifying the individual values of *J* and λ.

This problem is highlighted in Fig. 5 where the Swalen and Ibers potential is fitted up to τ = 34° constraining *J* at 1.5, 5.1, 15, and 50 eV. All of these fits describe the surface with some degree of success and depict similar values of $2J/\lambda$ from 0.66 to 0.93, yet the other parameters vary dramatically. Optimizing all 3 parameters leads to *J* = 5.5 eV and other results that are very similar to the ones obtained analytically based on just the well depth and angle and the ω_g/ω_i ratio. The figure also shows the results of optimizing all 3 parameters for the NH3-2010 surface, again determining values close to the analytical results. Table 2 lists these fully optimized results.

In a subsequent work,[106] we show that NH_3 is an atypical example of the XH_3 series as only for it is $2J/\lambda$ near unity. Also, we show that only for it is the lowest-energy Rydberg orbital lower in energy than the σ^*_{NH} orbital, an effect that greatly perturbs the diabatic model. Most significantly, that work also shows that, in any 3-parameter diabatic model for molecules of this type, the values of $\tau_m = \text{atan}(1/2) = 26.6°$ (or $\theta_m = \text{acos}(-1/5) = 101.5°$) are expected to be universal constants. Making this assumption then provides a unique method for diabatization of the ground-state surfaces *alone* to yield realistic estimates of excited-state transition energies.

3b. Application to calculated potential-energy surfaces for the ammonia inversion reaction

The origin of the ammonia double well is qualitatively described using even the simplest electronic-structure calculation methods. Valence-bond theory pertinent to the torsional motion identifies three key orbitals for NH_3:[83, 99, 133] the occupied symmetric NH bonding orbital σ_A, the occupied non-bonding p_z orbital *n*, which forms the highest-occupied molecular orbital (HOMO), and the unoccupied σ^*_A symmetric NH antibonding orbital. We find that complete-active-space self-consistent-field[134-136] (CASSCF) calculations depict the torsional potential

Cite this: DOI: 10.1039/c0xx00000x

www.rsc.org/xxxxxx

ARTICLE TYPE

Table 2. Diabatic-model parameters, as well as the resulting diabatic well depth $\Delta E^{\ddagger}$ and equilibrium torsional angle τ_e, fitted to the Swalen and Ibers[128] or NH3-2010[130] potentials based on experimental data, or else to CAS(2,2)/STO-3G or EOM-CCSD/STO-3G calculated data for NH_3 inversion.

Method	Adiab Cal[d]		Adiab fit		Diabatic model parameters															
	$\Delta E^{\ddagger}$	τ_e	$\Delta E^{\ddagger}$	τ_e	#[e]	J_G	J_D	λ_G	λ_D	$\frac{2\lvert J_G\rvert}{\lambda_G}$	$\frac{2\lvert J_D\rvert}{\lambda_D}$	k	k_4	γ_G	γ_D	τ_{mG}	τ_{mD}	α_G	α_D
	eV	°	eV	°		eV	eV	eV	eV			meV/°^{2}	meV/°^{4}	meV/°^{3}	meV/°^{3}	°	°	eV/°	eV/°
NH3-2010	0.22	22	0.22	22	3[a]	14.4	14.4	32.7	32.7	0.88	0.88	14.7	-	-	-	33.4	33.4	0.49	0.49
Swalen&Ibers	0.25	22	0.25	22	3[a]	5.5	5.5	13.6	13.6	0.80	0.80	9.2	-	-	-	26.5	26.5	0.25	0.25
CAS(2,2)	0.54	25	0.37	27	5[a]	6.05	7.62	14.3	26.2	0.85	0.58	10.73	-	-	-	25.8	35.0	0.277	0.375
CAS(2,2)	0.54	25	0.54	25	8[b]	6.09	7.64							-0.36	-1.09			0.22	0.28
CAS(2,2)	0.54	25	0.54	25	8[c]	6.09	7.64	18.0	32.1	0.67	0.49	7.51	-2	-0.29	-0.43	34.6	46.2	0.26	0.35
CAS(2,2)	0.54	25	0.54	23	8[a]	6.09	7.64	18.3	30.9	0.67	0.49	7.61	-6.7	-0.211	-0.363	34.7	45.1	0.264	0.343
EOM-CCSD	0.82	28	0.81	28	8[a]	5.87	7.12	19.8	36.9	0.59	0.39	6.27	13.4	-0.087	0.021	39.7	54.2	0.249	0.340

a: Fitted to potential-energy surface(s). b: Actual derivatives at D_{3h} structure. c: From anharmonicities at the D_{3h}, Eqn. (S8). d: Values from the original calculations or experimental potential. e: number of parameters in the fit.

well when just the two upper orbitals are included, however, indicating that σ_A is of secondary importance. Hence we exclude valence-bond structures involving this orbital, constructing a diabatic treatment that exploits variations in only the n and σ^*_A orbital occupancies only. This is the usual approach taken.[17, 137] In the minimal-basis set calculations that we present herein, the σ^*_A orbital is the LUMO but, when larger basis sets are used, Rydberg orbitals fall lower in energy.

Walsh diagram in Fig. 4 illustrates the properties of these orbitals. As the out-of-plane torsion angle τ increases, LUMO character strongly mixes into the HOMO in a continuous fashion,[138] significantly increasing the NH bond strengths and so lowering the molecular potential energy.[85, 137] It is this mixing process that defines the equilibrium geometry and hence hybridization and bonding in the molecule. Diabatic correlations for these orbitals are also shown in the figure. In a multi-state complete diabatic treatment, the orbital coefficients specifying the diabatic orbitals should not vary, but in few-state approaches such as this some variation is expected. The calculations show the diabatic orbitals to be the sketched *sp* hybridized orbitals on N mixed with some H *s* character. Differential mixing, when combined with the other bonding orbitals, generates the traditional sp^2 and sp^3 net hybridizations of the D_{3h} and equilibrium structures, respectively, but as the HNH bonding angle contracts below 90°, the lone-pair orbital takes on its diabatic *sp* form whilst the orthogonal bonding orbitals have the form $s^{1/2}p^{5/2}$.[138, 139] The significance of these properties of the diabatic orbitals is explored in detail elsewhere.[106]

The simplest calculation method that can deliver all states of interest is a CASSCF calculation involving 2 electrons in 2 orbitals, CAS(2,2), performed using a minimal basis set. Fig. 6 shows the adiabatic potential-energy surfaces for the ground state *g*, $n\rightarrow\sigma^*_A$ single excited state *s*, and $n\rightarrow\sigma^*_A$,$n\rightarrow\sigma^*_A$ doubly excited state *d* calculated using the STO-3G basis set.[140] At each molecular geometry, the NH bond length R is first optimized using second-order Mϕller-Plesset (MP2) perturbation theory.[141] All calculations are performed using MOLPRO.[142] In Fig. 6, the energies ΔE of each state relative to its energy in the D_{3h} geometry are plotted, allowing all three surfaces to be displayed on the same vertical scale. Shown also in this figure are representations of these surfaces using the 5-parameter and 8-parameter models. The 5-parameter model parameters are obtained by fitting the calculated energy surfaces, as is also done for the 8-parameter model. However, the 8-parameter model parameters are also obtained analytically from just calculated properties at the D_{3h} structure by either explicit derivative evaluation or else from interpreting anharmonicities, Eqn. (S8); MOLPRO evaluates the derivatives

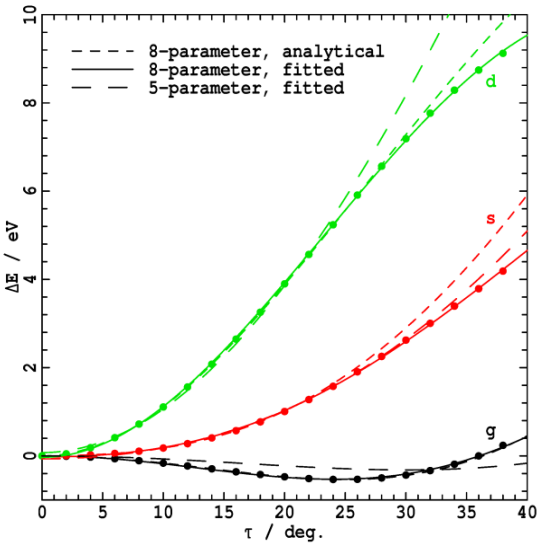

Fig. 6 The CAS(2,2)/STO-3G changes in adiabatic energies compared to those at the D_{3h} geometry for the ammonia inversion reaction (black: ground state *g*, red: HOMO→LUMO singly excited state *s*, green: HOMO→LUMO doubly excited state *d*) are plotted as a function of the torsional angle τ and fitted using various 3-state diabatic interaction models.

$$\alpha_G \approx \left\langle \psi_g \left| \frac{\partial H}{\partial \tau} \right| \psi_s \right\rangle \quad \text{and} \qquad \alpha_D \approx \left\langle \psi_s \left| \frac{\partial H}{\partial \tau} \right| \psi_d \right\rangle \tag{30}$$

analytically (a feature recently also now available for TD-DFT in

Q-CHEM)[143, 144] whilst the others are obtained by numerical differentiation:

$$\gamma_G = \frac{\partial^2}{\partial \tau^2}\alpha_G \quad \text{and} \quad \gamma_D = \frac{\partial^2}{\partial \tau^2}\alpha_D \,. \qquad (31)$$

Results are given in Table 2. For most properties the fit to the 5-parameter model works well but the equilibrium torsional angle of the ground state is overestimated by up to 5°. This anomaly is removed when the surfaces are fitted to all 8 parameters. Also, the values of the 8 parameters evaluated at $\tau = 0$ from either explicit derivatives or from interpreting anharmonicities are very similar to the ones fitted to the potential-energy surfaces, indicating that multi-mode effects such as the changes in the NH bond lengths that accompany torsional motion are not important. The diabatic model thus provides a realistic description of all potential-energy surfaces over a wide range of angle variation. Most significantly, it shows that, as is well known for electron-transfer processes,[104] ground-state structural properties can be determined from excited state spectra and vice versa, demonstrating the power of diabatic models.

Table 2 shows that the values of the parameters extracted from these fits are qualitatively similar to those determined from the 3-parameter fit to the Swalen and Ibers potential, but quite different to those from the NH3-2010 potential, owing to the instability in fitting experimental ground-state-only data discussed earlier. Also, the calculated well depths $\Delta E^{\ddagger}$ of 0.54 eV is far from the observed value of 0.220 eV. Table 2 also shows results evaluated using equations of motion coupled cluster theory (EOM-CCSD) [133, 134] using again the STO-3G basis, predicting an even larger well depth of 0.82 eV. In a subsequent work, we attribute this to the effects of Rydbergization,[106] finding that indeed the STO-3G results provide a realistic description of the valence-state properties compatible with those from high-level calculations.

3c. Application to proton transfer in $N_2H_7^+$.

Reactions involving the transfer of a proton, possibly coupled with electron transfer so that the net result is hydrogen-atom transfer, are extremely important biologically and are traditionally studied using coupled diabatic models.[52-59, 145] These reactions can involve a high degree of complexity as they could involve radical species and most often involve interfering reactions involving lone-pair orbitals on heavy atoms such as oxygen that are preserved in the reactant and product states but contribute significantly to transition states. So whilst proton-transfer at a simple level can be thought of as taking a proton away from one lone pair orbital and moving it to another, many interactions other than these may dominate observed processes. Also, while the basic process is described in terms of high-energy phenomena such as the breaking and making chemical bonds with hydrogen, the other interactions lead to low-energy transition states and weak effective couplings. Our focus here is not to investigate the manifold nature of general problems of current interest but rather on the basic underlying process of bond breakage and reformation, a diabatic process that is always present and always has influence.

We consider the protonated ammonia dimer, $N_2H_7^+$,

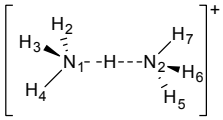

a closed-shell system that does not involve lone-pair orbitals other than those facilitating the fundamental chemical process. This makes this perhaps the simplest proton-transfer reaction.[146] We consider this reaction in the gas-phase only but this system also forms a model for significant processes observed in solution,[147] as well as for intramolecular proton transfer in molecules such as $NH_2CH_2CH_2CH_2NH_3^+$. Accurate gas-phase calculations require at least 6 nuclear degrees of freedom to be included,[146] but we shall focus on just the primary proton-transfer coordinate which has a_{2u} symmetry. This molecule has an apparent symmetric D_{3d} (NH_3-H^+-NH_3) structure that calculations indicate arises from a shallow double-well ground-state potential in the critical antisymmetric NH stretch coordinate which is too shallow to support zero-point vibration.[146, 148-150] The properties of the ground-state have been described using a vibronic coupling model involving diabatic states,[149] with 5 low-lying $^1A_{2u}$ Rydberg states interacting with the ground-state to produce its double-well potential-energy surface. This is a very practical diabatic analysis method focusing on observable states and dynamics, but the ground diabatic-state properties are fed into the analysis. Instead we focus on the fundamental interactions that give the ground-state those properties.

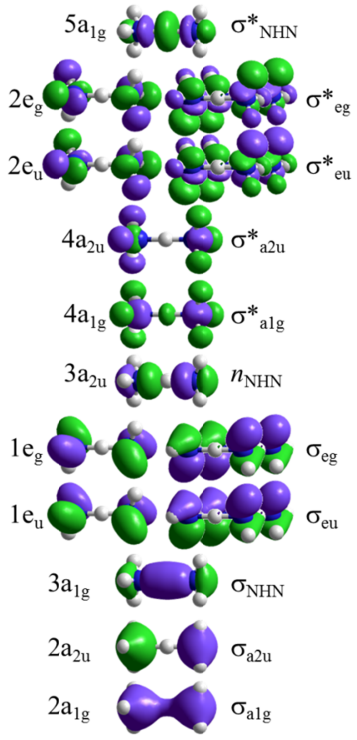

Fig. 7 Valence molecular orbitals for $N_2H_7^+$ at its symmetric D_{3d} structure; n_{NHN} is the HOMO orbital but it is the vibronic coupling between this and the highest unoccupied valence molecular orbital, σ^*_{NHN} that controls the ground-state symmetry.

Figure 7 shows the valence molecular orbitals of $N_2H_7^+$ at its symmetric D_{3d} structure. The most important orbitals affecting the ground-state structure are the non-bonding HOMO n_{NHN}, the occupied bonding orbital σ_{NHN}, and the unoccupied antibonding orbital σ^*_{NHN}. While only frontier orbitals control most chemical processes, here critical orbitals lie very low and very high in energy, with many other valence orbitals occurring in between. Indeed, σ^*_{NHN} is the highest *unoccupied* valence molecular orbital. In principle, all 3 orbitals are of equal significance but states rather than orbitals control properties. These states arise from either $n_{NHN} \rightarrow \sigma^*_{NHN}$ or else $\sigma_{NHN} \rightarrow \sigma^*_{NHN}$ excitation but the later are much higher in energy and therefore less important,[149] so we neglect them in this simple analysis. This makes the fundamental description of symmetry breaking in

$N_2H_7^+$ highly analogous to that in NH_3: both involve 3 orbitals at the valence-bond level including a low-lying doubly occupied orbital that is much less important than the others, leaving one occupied orbital and one virtual orbital to dominate the reaction profile. In both cases, the simplest robust diabatic model involves 3 intercoupled electronic states.

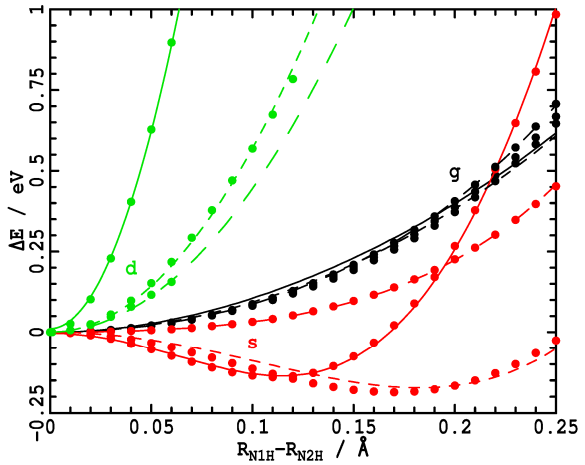

Fig. 8 Changes in adiabatic energies from those at the D_{3d} geometry for the *g* (black), *s* (red), and *d* (green) potential-energy surfaces of protonated ammonia dimer $N_2H_7^+$ as a function of the proton-transfer coordinate $\Delta R = R_{N1H} - R_{N2H}$, evaluated using the STO-3G basis by CAS(2,2) (solid lines), CAS(2,8) (short-dashed lines) and EOM-CCSD (long-dashed lines); points- raw calculated data, lines- adiabatic model fits to the data, see Table 3, (solid lines).

As for NH_3, the simplest calculation that includes all critical interacting states is CAS(2,2) in a minimal basis, and potential-energy surfaces calculated using the STO-3G minimal basis set are shown in Fig. 8. These surfaces are shown as a function of the asymmetry $R_{N1H-N2H}$ between the two shared NH bond lengths which replaces the generalized dimensionless normal coordinate Q used earlier. At each value of the asymmetry, all other variables are optimized at the MP2 level to minimize the energy of the ground state within the low-symmetry C_{3v} symmetry of the distorted molecule. This process is significant as the N-N distance changes somewhat during this distortion[149] and the resonance energy is sensitive to its value.[60, 151, 152] This imparts a strong non-Condon effect influencing the extended-model parameters β_G and β_D in ESI Eqns. (S5)-(S6), but the calculated potential-energy surfaces can be adequately fitted using the 5-parameter model that ignores this effect, as shown in the figure. The fitted parameters are given in Table 3.

Contrary to naive expectations, the ground-state surface shown in Fig. 8 has a single minimum whilst the singly-excited surface has a double minimum. This is interpreted as occurring because the associated resonance energies are not equivalent with J_G = 12.1 eV and J_D = 11.3 eV but more significantly the vibronic coupling is much stronger to *D* as λ_G = 21 eV and λ_D = 48 eV. While the properties of the doubly excited state appear to be paired with those of the ground state, the properties of the singly excited state depends intricately on the differential coupling to the other two. Most significantly, Table 2 indicates that $2J_G / \lambda_G$ = 1.04, very close to the critical value of unity for changeover between single-well and double-well behavior of the ground state and hence this system is expected to be very sensitive to changes in calculation type and molecular environment.

Figure 8 and Table 3 also include results for higher-level calculations, but still with the STO-3G basis to avoid complications with Rydberg states. These methods are CAS(2,8), in which all unoccupied valence orbitals are included, and EOM-CCSD, which includes all orbitals but at a simplified level that preferentially treats the ground-state compared to the singly and especially doubly excited states. The shapes of the excited-state potential-energy surfaces change considerably and the vibronic coupling is much reduced in magnitude. Clearly all orbitals need to be included in accurate calculations. Rydberg states may also interact with the intrinsic valence-state process. Even small changes to this system can be very important, however, as most molecular properties become extremely sensitive when $2J / \lambda \approx 1$. An example of this effect is that MP2/aug-cc-pVTZ[153] predict a very shallow ground-state double minimum,[150] and one sees similar effects when using different density functionals in Density Functional Theory.[154]

Obtaining accurate parameters for $N_2H_7^+$ will require significant effort owing to interference between the valence states of interest and Rydberg states. As an indication of the likely space in which such parameters should lie, EOM-CCSD/6-311++G** surfaces were evaluated and the effective 2-state model applied. This yielded J = 4.8 eV, λ = 10.2 eV, and $2J/\lambda$ = 1.05. The ground-state potential at this level of theory continues to have a delocalized hydrogen bond, but the control ratio is so close to unity that slight variations in the computational method could yield alternate results.

5. Closed-shell species with doubly degenerate HOMO and LUMO orbitals.

The results presented so far have used the assumption that the key chemical process controlling isomerization involves the mixing of just two primary valence orbitals, one occupied and one unoccupied. However, in many systems the key orbitals are either doubly degenerate or nearly so, with classic examples including benzene, naphthalene and other acenes, porphyrins and chlorophylls. For these systems, the HOMO to LUMO transition has the same symmetry as the second-highest occupied molecular orbital (SHOMO) to second-lowest unoccupied molecular orbital (SLUMO) transition, so that all vibronic couplings between these orbitals contribute to the observed ground-state and spectroscopic properties.

We consider vibronic coupling between the e_{1g} HOMO and the e_{2u} LUMO in benzene as a classic example of this type of interaction. The lowest excited electronic state has $^1B_{1u}$ symmetry and undergoes strong vibronic coupling involving[155-159] ν_{14}, a mode of $1b_{1u}$ symmetry, which is observed at 1309 cm^{-1} in the ground state[160] and 1563 cm^{-1} in the first excited state.[155, 161] Evoking Eqn. (15), the broader significance of this vibronic coupling has been recognized and $^1B_{1u}$ historically identified as the "twin state" of the ground state.[72-74] Distorting along this vibrational mode mixes the HOMO and LUMO orbitals to convert delocalized aromatic benzene into its two localized Kekulé structures representing the two cyclohexatriene molecules, directly akin to the effects of the ammonia inversion vibration. This distortion maintains the doubly degeneracy of the HOMO and LUMO orbitals which both adopt e" symmetry at distorted D_{3h} structures.

We depict the Kekulé distortion using the distortion angle ϕ shown in Fig. 9. This distortion produces structures with alternating short and long CC bond lengths given by

$$r_s = 2r_c \sin(30 - \phi) \quad \text{and} \quad r_l = 2r_c \sin(30 + \phi) , \qquad (32)$$

respectively. In all calculation, r_c as well as the two independent variables that determine the in-plane hydrogen coordinates are

Table 3. Diabatic-model parameters calculated data symmetry breaking for the proton-transfer process in $N_2H_7^+$, evaluates using the STO-3G basis.

Method	No. Params	J_G	J_D	λ_G	λ_D	$\frac{2\lvert J_G\rvert}{\lambda_G}$	$\frac{2\lvert J_D\rvert}{\lambda_D}$	$\Delta E^{\ddagger}$	k	k_4	δ_G	δ_D	α_G	α_D
		eV	eV	eV	eV			eV	eV/Å^2	eV/Å^4	Å	Å	eV/Å	eV/Å
CAS(2,2)	5	12.1	11.3	20.8	48.3	1.16	0.47	0	157.5	[0]	0.26	0.39	40.5	61.7
CAS(2,8)	6	8.7	8.9	8.8	37.1	1.98	0.48	0	37.2	-0.04	0.34	0.71	12.8	26.3
EOM-CCSD	6	7.9	8.9	8.6	25.3	1.83	0.71	0	36.6	1.19	0.34	0.59	12.6	21.5

optimized using MP2/6-31G* at each value of ϕ. The resulting bond-length alternation is found to increase nearly linearly with angle, with $(r_l - r_s)/\phi \approx 0.042$ Å/°. A distortion of $\phi = \pm 2.6°$ creates alternating bond lengths of 1.31 Å and 1.53 Å, as would naively be expected for isolated single and double bonds, whilst $\phi = \pm 1.1°$ creates a structure with bond-length alternation typical of that expected for a cyclohexatriene-like Kekulé structure.[162] The effective mass (really a moment of inertia) associated from this motion deduced from the optimized structures is μ = 0.6037 amu Å^2. Note that this procedure generates potential-energy surfaces as a function of a curvilinear coordinate, as is essential say for modeling ammonia inversion; however, the distortions for benzene are so small that the alternate use of a normal coordinate, which treats explicitly the significant mixing between the carbon and hydrogen bending motions,[157] may be more appropriate.

As shown in Fig. 2, benzene can sustain four analogous promotions of an electron from its HOMO to its LUMO, generating 7 strongly coupled delocalized diabatic electronic states: the ground state G, the single excitation of $^1B_{1u}$ symmetry S, three independent doubly excited ^1A_g states D_1, D_2, and D_3, a triple excitation T of $^1B_{1u}$ symmetry, and quadruple excitation Q of ^1A_g symmetry. A simple analytical model for these interactions can be constructed on the assumptions that the three double excitations can be replaced by a single effective excitation, that the remaining 5 states are equally coupled to each other, and that the two-electron repulsion integrals are invariant to the electron distribution within the HOMO and LUMO. In the electronic basis set $\{\psi_G, \psi_S, \psi_D, \psi_T, \psi_Q\}$ this produces the 3-parameter delocalized diabatic Hamiltonian $\mathbf{H}^{5D}$ =

$$\begin{bmatrix} H_\phi & \alpha\phi & 0 & 0 & 0 \\ \alpha\phi & H_\phi + 2J & \alpha\phi & 0 & 0 \\ 0 & \alpha\phi & H_\phi + 4J & \alpha\phi & 0 \\ 0 & 0 & \alpha\phi & H_\phi + 6J & \alpha\phi \\ 0 & 0 & 0 & \alpha\phi & H_\phi + 8J \end{bmatrix} \quad (33)$$

where $H_\phi = T + k\phi^2/2$. The eigenvalues of this matrix give the adiabatic surfaces

$$\begin{aligned} \varepsilon_g &= \frac{k}{2}\phi^2 + 4J - \left[2\alpha^2\phi^2 + 10J^2 + E_x\right]^{1/2} \\ \varepsilon_s &= \frac{k}{2}\phi^2 + 4J - \left[2\alpha^2\phi^2 + 10J^2 - E_x\right]^{1/2}, \\ \varepsilon_d &= \frac{k}{2}\phi^2 + 4J, \\ \varepsilon_t &= \frac{k}{2}\phi^2 + 4J + \left[2\alpha^2\phi^2 + 10J^2 - E_x\right]^{1/2}, \text{ and} \\ \varepsilon_q &= \frac{k}{2}\phi^2 + 4J + \left[2\alpha^2\phi^2 + 10J^2 + E_x\right]^{1/2} \text{ where} \\ E_x &= (\alpha^4\phi^4 + 24\alpha^2\phi^2J^2 + 36J^4)^{1/2}. \end{aligned} \quad (34)$$

Hence there is a close relationship between the ground-state g and the quadruple excitation q, as well as a close relationship between the single excitation s and the triple excitation t. Equation (34) is similar to Eqn. (4) but not quite of the same form, so it is not immediately clear if these paired states are twins according to our definition or not. Generally, from the second derivatives of these adiabatic potential-energy surfaces at $\phi = 0$, the expected adiabatic vibration frequencies are

$$\begin{aligned} \omega_i &= \omega\left(1 - \frac{\lambda}{2|J|}\right)^{1/2}, \\ \omega_s &= \omega_d = \omega_t = \omega, \text{ and} \\ \omega_q &= \omega\left(1 + \frac{\lambda}{2|J|}\right)^{1/2} \end{aligned} \quad (35)$$

where $\lambda = 2\alpha^2/k$. These results directly parallel the classic one electron/hole in two orbitals scenario (Eqn. (6) and (7)) and the two-electrons in two-orbitals scenario (Eqn. (27)), suggesting that g and d are approximately twinned. Indeed, for small angle motions of systems with strong coupling, $(\alpha\phi/J)^4$ can be ignored so that $E_x = (\alpha^4\phi^4 + 24\alpha^2\phi^2J^2 + 36J^4)^{1/2} \sim 6J^2 + 2\alpha^2\phi^2$ and the eigenvalues for the ground state and quadruple excitation become

$$\begin{aligned} \varepsilon_g &\approx \frac{k\phi^2}{2} + 4J - \left(16J^2 + 4\alpha^2\phi^2\right)^{1/2} \\ \varepsilon_q &\approx \frac{k\phi^2}{2} + 4J + \left(16J^2 + 4\alpha^2\phi^2\right)^{1/2}. \end{aligned} \quad (36)$$

These adiabatic surfaces do indeed have to from of Eqn. (4) and hence g and q are listed as "twin states" in Table 1. To be written in the form $\varepsilon_\pm(Q) = kQ^2/2 + J' \mp (J'^2 + \alpha'^2Q^2)^{1/2}$, the fundamental parameters appearing in Eqn. (36) must be renormalized according to J'=4J, λ'=4λ, α'=2α, and ϕ'_m=2 ϕ_m where $\phi_m = \alpha/k$. As for the two-electrons in two-orbitals case (Eqn. (22)), the critical ratio $2J/\lambda$ remains preserved, however.

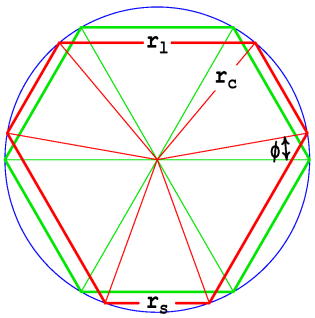

Fig. 9 Definition of the angle ϕ (shown here at 10°) and the radius r_c (shown here angle independent for simplicity) used for the description of the $^1b_{1u}$ Kekulé distortion of benzene, producing short and long CC bond lengths r_s and r_l, respectively.

Also, the small-angle approximation leads to the conclusion that *s* and *t* are also twinned states, though the potential-energy surfaces are basically undistorted from their diabatic limits. Later we demonstrate that the small-angle scenario is appropriate for benzene at any angle normally considered in spectroscopic studies.

Alternatively, Eqn. (34) may be investigated in the large angle (or small coupling) scenario in which the contribution $\alpha^4\phi^4$ may be neglected, leading to $E_x = (\alpha^4\phi^4 + 24\alpha^2\phi^2J^2 + 36J^4)^{1/2} \sim \alpha^2\phi^2 + 12J^2$. The pair *g* and *d*, as well as the pair *s* and *t*, again appear twinned, but the renormalization is different, see Table 1. The properties of the system in this regime are most clearly revealed by applying the rotation $\mathbf{H^{5L}} = \mathbf{R}\mathbf{H^{5D}}\mathbf{R}^{\mathrm{T}}$ to produce in the localized diabatic electronic basis set $\{\psi_{LL},\psi_L,\psi_C,\psi_R,\psi_{RR}\}$, obtaining the Hamiltonian $\mathbf{H^{5L}}$ =

$$\begin{bmatrix} H_0(-\sqrt{3},3) & J+\frac{2J}{\sqrt{3}} & 0 & J-\frac{2J}{\sqrt{3}} & 0 \\ J+\frac{2J}{\sqrt{3}} & H_0(-1,1) & \frac{-4J}{\sqrt{3}} & 0 & -J+\frac{2J}{\sqrt{3}} \\ 0 & \frac{-4J}{\sqrt{3}} & H_0(0,0) & \frac{4J}{\sqrt{3}} & 0 \\ J-\frac{2J}{\sqrt{3}} & 0 & \frac{4J}{\sqrt{3}} & H_0(1,1) & -J-\frac{2J}{\sqrt{3}} \\ 0 & -J+\frac{2J}{\sqrt{3}} & 0 & -J-\frac{2J}{\sqrt{3}} & H_0(\sqrt{3},3) \end{bmatrix} \quad (37)$$

where $H_0(x,y) = T + k(\phi - x\phi_m)^2/2 - y\lambda/4$ and

$$R = \begin{bmatrix} \frac{1}{2\sqrt{3}} & \frac{1}{2} & \frac{1}{\sqrt{3}} & \frac{1}{2} & \frac{1}{2\sqrt{3}} \\ \frac{-1}{2} & \frac{-1}{2} & 0 & \frac{1}{2} & \frac{1}{2} \\ \frac{-1}{\sqrt{3}} & 0 & \frac{1}{\sqrt{3}} & 0 & \frac{-1}{2\sqrt{3}} \\ \frac{1}{2} & \frac{-1}{2} & 0 & \frac{1}{2} & \frac{-1}{2} \\ \frac{1}{2\sqrt{3}} & \frac{-1}{2} & \frac{1}{\sqrt{3}} & \frac{-1}{2} & \frac{1}{2\sqrt{3}} \end{bmatrix}. \quad (38)$$

This reveals that the fully localized diabatic surfaces (i.e., those for *J*=0) comprise two sets of double wells, a deep pair (*LL* and *RR*) with minima at $\phi = \pm\sqrt{3}\phi_m$ and a shallow pair (*L* and *R*) with minima at $\varphi = \pm\phi_m$. The deep set form the twinned adiabatic ground state and quadrupally excited whilst the shallow set form the twinned singly excited and triply excited states.

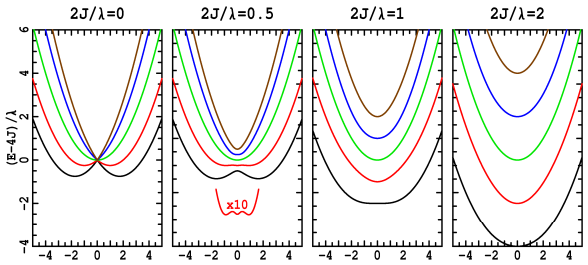

Fig. 10 Sample adiabatic potential-energy surfaces (black- *g*, red- *s*, green- *d*, blue- *t*, brown- *q*) from the 5-state model for the Kekulé distortion of benzene, Eqn. (34).

Fig. 10 puts the low-angle and high-angle limits together, showing the shapes of the adiabatic states (Eqn. 34) that form for $2J/\lambda = 0$, 0.5, 1, and 2. The ground-state is double-welled if $2|J|/\lambda < 1$ but in this region the singly excited state is triple welled, having both a local minimum at the D_{6h} geometry and local minima at distorted geometries. The properties of this state are thus very complex indeed.

However, the previous analysis is based on the assumption that the couplings between the different electronic states are all equal. This is unlikely to be true in practice, as demonstrated earlier for the simpler problem of ammonia inversion. Indeed, three different variants of the double excitation arise, making the scenario for benzene quite complex. The simplest model that semiquantitatively describes all features of the Kekulé distortion of benzene is therefore the 7-state model

$$\mathbf{H^{7D}} = \begin{bmatrix} T+\frac{k}{2}\phi^2 & \alpha_{GS}\phi & & & & & \\ \alpha_{GS}\phi & T+\frac{k}{2}\phi^2+E_S & \alpha_{SD1}\phi & \alpha_{SD2}\phi & \alpha_{SD3}\phi & & \\ & \alpha_{SD1}\phi & T+\frac{k}{2}\phi^2+E_{D1} & & & \alpha_{D1T}\phi & \\ & \alpha_{SD2}\phi & & T+\frac{k}{2}\phi^2+E_{D2} & & \alpha_{D2T}\phi & \\ & \alpha_{SD3}\phi & & & T+\frac{k}{2}\phi^2+E_{D3} & \alpha_{D3T}\phi & \\ & & \alpha_{D1T}\phi & \alpha_{D2T}\phi & \alpha_{D3T}\phi & T+\frac{k}{2}\phi^2+E_t & \alpha_{TQ}\phi \\ & & & & & \alpha_{TQ}\phi & T+\frac{k}{2}\phi^2+E_Q \end{bmatrix}. \quad (39)$$

Cite this: DOI: 10.1039/c0xx00000x

www.rsc.org/xxxxxx

ARTICLE TYPE

Table 4. Properties and diabatic-state model parameters for the Kekulé distortion in benzene.

Prop.[a]	CAS(4,4) @ D_{6h}	CAS(4,4) best fit	NEVPT2 best fit	NEVPT2 poor fit	Exp.
$2J_G$	7.2	7.2	5.08	5.08	4.77
E_{D1}	12.6	12.6	10.49	10.49	[9.54]
E_{D2}	14.8	14.8	-	-	-
E_{D3}	20.3	20.3	-	-	-
E_T	22.3	22.3	[15.73]	[15.73]	[14.31]
E_G	32.1	32.1	[20.97]	[20.97]	[19.08]
α_{GS}	0.96	0.77	0.70	0.52	0.55
α_{SD1}	0.52	0.38	0.70	0.40	[0.55]
α_{SD2}	0.98	0.79	-	-	-
α_{SD3}	0.02	0.42	-	-	-
α_{D1T}	0.61	0.38	1.05	0.75	[0.55]
α_{D2T}	0.66	0.29	-	-	-
α_{D3T}	0.58	0.56	-	-	-
α_{TQ}	0.66	0.31	[0.70]	[0.52]	[0.55]
K		0.658	0.489	0.165	0.429
λ_G		1.81	2.00	1.31	[1.43]
ϕ_{mG}		1.17	1.43	[1.25]	[1.29]
$2J_G/\lambda_G$		4.00	2.55	3.88	[3.34]
J_G'[b]		16.1	10.48	10.48	[9.54]
λ_G'[b]		5.62	7.44	4.73	5.71
ϕ_{mG}'[b]		2.08	2.57	2.37	2.58
$2J_G'/\lambda_G'$		5.73	2.82	4.43	3.34
ω_i		1678	1304	970	1309
ω_s		1825	1626	1191	1564

[a] energies E, J, and λ in eV, vibronic coupling constants α in eV/°, force constants k in eV/°^{2}, diabatic angle minima ϕ_m in °, vibrational frequencies ω in cm^{-1}.

[b] calculated values determined from α's setting all E's to zero in the model and using $3\lambda_g'=4\lambda_g''$ and $2\phi_{mG}'=3^{1/2}\phi_{mG}''$; fitting directly to the ground-state surface yields J_G'= 11.8 eV, λ_G'= 6.36 eV, ϕ_{mG}'= 3.07°, and $2J_G'/\lambda_G'$ = 3.71 for CAS(4,4) but the NEVPT2 surfaces are too harmonic too allow such fitting.

The simplest calculation that can manifest all of the quantities in this model is CAS(4,4). Evaluated directly by MOLPRO at the D_{6h} ground-state structure using the 6-31G* basis set, the calculated vibronic coupling constants, included in Table 4, are α_{GS} = 0.96 eV/°, α_{SD1} = 0.52 eV/°, α_{SD2} = 0.98 eV/°, α_{SD3} = 0.02 eV/°, α_{D1T} = 0.61 eV/°, α_{D2T} = 0.66 eV/°, α_{D3T} = 0.58 eV/°, and α_{TQ} = 0.66 eV/°. All of the states are thus interact with each other quite strongly, as the simple 3-parameter model depicts, but there are considerable variations indicated and the three components of the double excitation have non-trivial interactions. This model has in total 15 parameters depicting the properties of the 7 states: 8 vibronic coupling constants, 6 energy differences at the D_{6h} structure, and the force constant k.

Optimizing all parameters to fit the calculated potential-energy surfaces results in some changes to the actual derivatives but the basic scenario remains the same; the fitted parameters are also given in Table 4 whilst the calculated potential-energy surfaces and their fits are shown in Fig. 11. The splitting of the double excitation into three well-separated components influences on the properties of the single excitation and the triple excitation as energy gaps get reduced. As a result, the naïve dispersion of the vibration frequencies of the states depicted by Eqn. (35) is destroyed, with the state of lowest frequency becoming a component of the double excitation while the triple excitation becoming that of highest frequency. By setting to zero all of the energy gaps in the Hamiltonian, a lower adiabatic surface can be obtained whose properties mimic those that would be used in an effective two-state localized diabatic model, allowing effective parameters λ_G' and ϕ_{mG}' to be determined, along with $2J_G$ ' from the energy of the quadrupally excited state. If the critical conclusion deduced from Eqn. (35), that the quadruple excitation is the "twin state" to the ground state, remains valid, then one expects to find $\lambda_G' = 4\lambda_G$ and $\phi_{mG}' = 2\phi_{mG}$ with the ratio of $2J_G'/\lambda_G' = 2J_G/\lambda_G$ preserved. Deduced values for these quantities

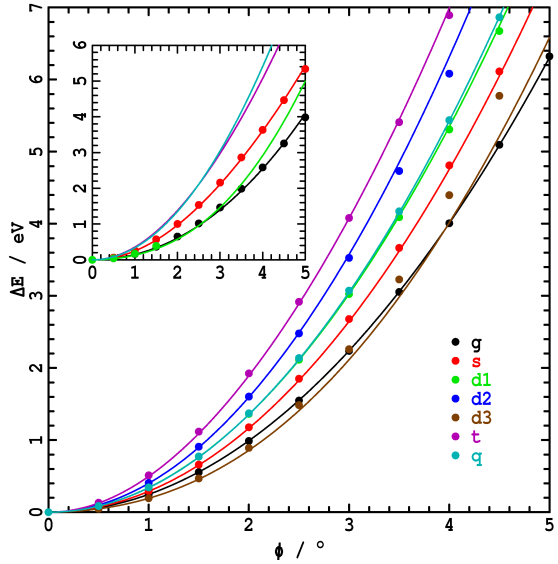

Fig. 11 Calculated (points) and diabatic-model fitted (lines) adiabatic potential-energy surfaces, expressed relative to the energy at the D_{6h} symmetric structure given in Table 4, for the various coupled HOMO→LUMO multiple excitations of benzene as a function of the Kekulé distortion angle ϕ (see Figs. 2 and 8). The main plot shows results at the CAS(4,4)/6-31G* level whilst the insert shows those after second-order perturbation-theory correction, NEVPT2.

shown in Table 2 do indeed show results similar to that expected, although $2J_G/\lambda_G$ = 4.0 whilst $2J_G'/\lambda_G'$ = 5.7. The twin-state concept thus appears to remain useful, despite the manifest strong interactions between the singly excited state, the triply excited state, and all the double excitations.

The CAS(4,4) method lacks quantitative accuracy, however, with for example the energy of the single excitation being predicted to be 7.2 eV compared to 4.77 eV observed, whilst the calculated ground-state and single-excited state frequencies are predicted to be 1678 cm^{-1} and 1825 cm^{-1}, much larger than the observed values of 1309 cm^{-1} and 1564 cm^{-1}, respectively. We therefore performed enhanced calculations using the n-electron valence-state implementation of second-order multireference perturbation theory (NEVPT2).[163] Owing to likely degeneracies

of the 7 states of interest with other states, this method is not universally applicable and is likely to overestimate effects, particularly for excited states. However, potential-energy surfaces for the ground state, singly excited state, and first component with double excitation were obtained and are shown in Fig. 11. As the remaining surfaces were not determined, an unconstrained fit of all parameters in the model is not possible. We proceed by ignoring the other two components of the double excitation and setting the parameters of the triple excitation and quadruple excitation to match those fitted to the other surfaces in a pseudo 3-parameter model.

The results, shown in the figure and in Table 3, manifest a considerable reduction in the force constant and some variation in the vibronic coupling constants. The deduced ground state vibration frequency thus reduces to ω_i = 1304 cm^{-1}, in excellent agreement with the experimental value, while ω_s = 1626 cm^{-1} is now underestimated. In addition, the diabatic angle for an effective two-state model becomes ϕ_{mG}' = 2.57°, indicating diabatic single-bond and double-bond lengths of 1.53 Å and 1.31 Å, respectively, in excellent agreement with the properties of isolated CC bonds. Finally, the critical ratios depicting the coupled diabatic interactions become $2J_G/\lambda_G$ = 2.55 and $2J_G'/\lambda_G'$ = 2.82, indicating that the explicit inclusion of the *S* and *D1* intermediate states has not significantly perturbed the simple picture of the quadruple excitation being the "twin state" of the ground state.

Results are also shown in Table 3 for a second, much poorer quality, fit to the NEVPT2 calculated data in which ϕ_{mG} was modified from its optimized value of 1.43° to 1.25°. The diabatic couplings are found to be very sensitive to this parameter, with in particular the coupling ratio α_{SD1}/α_{GS} being reduced in a way which would isolate the ground-state and singly excited state from the other transitions and in so doing potentially identify the single excitation as the "twin state" of the ground state, as has been previously proposed.[72-74] However, even after this significant perturbation, the fitting still indicates that the twin state is the quadruple excitation. The analysis is therefore robust.

Only a limited amount of experimental information concerning the state manifold is available, and so gross approximations must be introduced to estimate diabatic-coupling parameters. Progress can only be made if the 3-parameter model is introduced. Using this, Eqn. (35) indicates that $2J_G'/\lambda_G'$ = 3.34, in reasonable agreement with the NEVPT2 results. Also J_G = 2.38 eV is determined by the observed transition energy for the single excitation, so that given the reduced mass for the torsional motion optimized at the MP2/6-31G* level all other diabatic properties can be deduced (see Table 3). All are in good qualitative agreement with the NEVPT2 results, including the important two-state localized-diabatic distortion angle ϕ_{mG}' = 2.58°.

6. Conclusions

While diabatic models for general chemical processes have been suggested since the quantum foundations of chemistry were first established, we present a robust formalism that is suitable for quantitative analysis of general chemical reactions. It is based on London's model for non-adiabatic reactions[10] as implemented in Hush's adiabatic-based description of electron-transfer reactions and spectroscopy.[100-104] Direct analogies to well understood electron-transfer problems are established that allow many seemingly unrelated properties of the ground state and excited state potential-energy surfaces to be correlated, describing complex surfaces in terms of simple functions.

This treatment breaks from previous partially successful approaches to expressing general reactions in diabatic bases in that all electronic states coupled by the critical vibronic coupling constants are included. While these earlier approaches focused on identifying just two states so that a direct analogy to electron-transfer and pseudo Jahn-Teller processes could be drawn,[19, 71-74, 98] our multi-state approach leads to the conclusion that two-state models can be qualitatively descriptive but that the parameters in them are renormalized from the actual molecular parameters, and that this renormalization depends on the property being investigated. Critical previous ideas such as the notion[71-74] of a "twin state" with properties intimately linked to those of the ground state are established, identifying the actual nature of the twin state. Also, previous conclusions[13-19] concerning the importance of pseudo-Jahn-Teller processes and their symmetry are fully vindicated, but we see now that more than two states are fundamentally involved meaning that more than one conical intersection has profound effects on structure and spectroscopy.

The general procedure is applied to 3 illustrative cases, ignoring complications like electronic interactions and also conical intersections with Rydberg states that in practice dominate most relevant spectroscopic measurements, photodissociation processes and theoretical analyses. Consistent, simple descriptions are obtained for the inversion reaction in ammonia, the intramolecular proton-transfer reaction in $N_2H_7^+$, and the Kekulé motion of benzene that is associated with its aromaticity. Major qualitative changes such as the change of the ground state from high-symmetry to a symmetry-broken geometry are seen to result from small changes in the diabatic-model parameters, and these are correlated with spectroscopic transition energies and the shapes of excited-state surfaces. What results is a simple semi-quantitative description of the chemistry and spectroscopy of these different processes using a consistent language and notation.

Undergraduate teaching of the basic principles of chemistry often focuses on reactions of the type considered, describing the results in terms of *independent* chemical principles describing, e.g., hybridization, general isomerization reactions, VSEPR, aromaticity in benzene, hydrogen bonding, and electron transfer. Here we present the basic science underlining a different approach based on diabatic surfaces and the drives for localization and delocalization of electrons. This approach flows smoothly from the basic understanding of covalent bonds and how they form,[164-166] as well as linking to ionic and metallic bonding, as well as to electron-transfer processes critical in many modern applications in biochemistry, solar-energy capture, and molecular electronics. It builds a connection between basic qualitative ideas, experimental data interpretation, and ab initio calculations.

Appendix: Mathematical symbols used

Variable Class	Description	Variations
Q, τ, ΔR, ϕ	Nuclear coordinate	Q – dimensionless normal coordinate used to represent the nuclear motion $\pm Q_m$ – location of the minima in the diabatic surfaces for electron transfer $\pm Q_{mG}$, Q_{mG} – location of the minima in the diabatic surfaces for the 2-electron in 2-orbitals problem $\pm Q_m'$ – apparent location of the minima in the diabatic surfaces for an effective 2-state model Q_e – minimum of the adiabatic surface **Substitutions:** $Q \rightarrow \tau$ - the improper torsional angle for NH_3 inversion, related to HNH bond angle θ by Eqn. (28) $Q \rightarrow \Delta R = R_{N1H} - R_{N2H}$ for proton transfer in $N_2H_7^+$ $Q \rightarrow \phi$, the Kekulé angle distortion for benzene aromaticity
$\mathbf{H}$	Electronic Hamiltonian matrix	$\mathbf{H}^{\mathbf{2D}}$ - expressed in basis of delocalized diabatic states $\{G,S\}$ depicting the ground state (G), and single excited state (S) for an electron-transfer problem $\mathbf{H}^{\mathbf{2L}}$ - expressed in basis of localized diabatic states $\{L,R\}$ centred on the L (left) and R (right) molecular centres in an electron-transfer problem. $\mathbf{H}^{\mathbf{3D}}$ - expressed in basis of delocalized diabatic states $\{G,S,D\}$ depicting the ground state (G), single excited state (S), and double excited state (D). $\mathbf{H}^{\mathbf{3L}}$ - expressed in basis of localized diabatic states $\{L,C,R\}$ centred on the L (left) isomer, C (central) high-symmetry structure, and R (right) isomer. $\mathbf{H}^{\mathbf{5D}}$, $\mathbf{H}^{\mathbf{5L}}$, $\mathbf{H}^{\mathbf{7D}}$ - 5-state and 7-state variants for the HOMO-LUMO excitations in benzene
J	Resonance integral	J - electronic coupling in an electron-transfer problem J_G, J_D - this generalized to a two-electron in 2-orbital problem, specifying the magnitude of the energy differences between S and the G and D states J' - apparent coupling used in an effective 2-state model
λ	Reorganisation energy	λ - reorganization energy in an electron-transfer problem λ_G, λ_D - this generalized to a two-electron in 2-orbital problem, applied to excitations between S and the G and D states λ' - apparent reorganization energy used in an effective 2-state model
$2J/\lambda$	General ratio controlling properties of diabatic model Hamiltonians	$2J/\lambda$ for an electron-transfer problem $2J_G/\lambda_G$ and $2J_D/\lambda_D$ - this generalized to the individual components of a 2-orbital e-electron problem $2J'/\lambda'$ - apparent ratio in an effective two-state model
μ'	Effective mass	
k	Harmonic force constant	
k_4	Quartic force constant	Used only for the large amplitude torsional bending in NH_3
$\lvert\Psi\rangle$	Electronic state wavefunction	$\lvert\Psi_G\rangle$, $\lvert\Psi_S\rangle$, $\lvert\Psi_D\rangle$ describing the diabatic states
α	Linear vibronic coupling constant	$\alpha = \langle\Psi_G \lvert \partial\mathbf{H}/\partial Q \rvert \Psi_S\rangle\rvert_{Q=0}$ for electron transfer $\alpha_G = \langle\Psi_G \lvert \partial\mathbf{H}/\partial Q \rvert \Psi_S\rangle\rvert_{Q=0}$ for 2-electrons in 2-orbitals $\alpha_D = \langle\Psi_D \lvert \partial\mathbf{H}/\partial Q \rvert \Psi_S\rangle\rvert_{Q=0}$ for 2-electrons in 2-orbitals α' - apparent vibronic coupling active in an effective two-state model
γ	Cubic vibronic coupling constant	$\gamma_G = \langle\Psi_G \lvert \partial^3\mathbf{H}/\partial Q^3 \rvert \Psi_S\rangle\rvert_{Q=0}$ $\gamma_D = \langle\Psi_D \lvert \partial^3\mathbf{H}/\partial Q^3 \rvert \Psi_S\rangle\rvert_{Q=0}$
ε	Adiabatic surfaces	ε_g, ε_s, ε_d, ε_t, ε_q - ground state, singly excited, double excited, triply excited and quadruply excited surfaces
ω	Vibration frequency	ω - vibration frequency of the diabatic states $\omega_g, \omega_s, \omega_d$ - vibration frequency of the adiabatic ground, single excited, and doubly excited states ω_i - imaginary vibration frequency of the transition state
$\Delta E^{\ddagger}$	Activation energy	
r	Bond lengths	r_s, r_c, r_l - lengths of double, aromatic, and single CC bonds, respectively

Acknowledgments

We thank the Australian Research Council Discovery Projects scheme for funding this research and National Computational Infrastructure (NCI) for the provision of computational resources.

Notes and references

a: International Centre for Quantum and Molecular Structure, College of Sciences, Shanghai University, Shanghai 200444 China; Tel: 86-15618155341; E-mail: Jeffrey.Reimers@uts.edu.au
b: School of Mathematical and Physical Sciences, University of Technology Sydney, NSW 2007 Australia
c: Department of Physics and Astronomy, University College London, Gower Street, London WC1E 6BT UK
d: School of Chemistry, The University of Sydney, Sydney, NSW 2006 Australia
e: School of Mathematics and Physics, The University of Queensland, QLD 4072 Australia
f: School of Molecular Biosciences, The University of Sydney, NSW, 2006 Australia

† Electronic Supporting Information (ESI) available: xxxxx. See DOI: xxxxxxxxxxxxxx

1. M. Born and R. Oppenheimer, *Ann. Phys.*, 1927, **84**, 457.
2. T. Van Voorhis, T. Kowalczyk, B. Kaduk, L.-P. Wang, C.-L. Cheng and Q. Wu, *Annu. Rev. Phys. Chem.*, 2010, **61**, 149.
3. E. J. Barton, C. Chiu, S. Golpayegani, S. N. Yurchenko, J. Tennyson, D. J. Frohman and P. F. Bernath, *Mon. Not. R. Astron. Soc.*, 2014, **442**, 1821.
4. F. London, *Z. Phys.*, 1928, **46**, 455.
5. H. Eyring and M. Polanyi, *Z. Phys. Chem. Abt. B*, 1931, **12**, 279.
6. M. G. Evans and M. Polanyi, *Trans. Faraday Soc.*, 1938, **34**, 11.
7. J. Horiuti and M. Polanyi, *J. Molec. Catalysis A*, 2003, **199**, 185. Translation of *Acta Physicochimica U.R.S.S.* 1935, **2**, 505–532.
8. F. T. Wall and G. Glockler, *J. Chem. Phys.*, 1937, **5**, 314.
9. N. S. Hush, *J. Polym. Sci.*, 1953, **11**, 289.
10. F. London, *Z. Phys.*, 1932, **74**, 143.
11. L. D. Landau, *Z. Phys. Sowjetunion*, 1932, **2**, 46.
12. L. D. Landau, *Z. Phys. Sowjetunion*, 1932, **1**, 88.
13. R. F. W. Bader, *Can. J. Chem.*, 1962, **40**, 1164.
14. L. Salem and J. S. Wright, *J. Amer. Chem. Soc.*, 1969, **91**, 5947.
15. R. G. Pearson, *J. Amer. Chem. Soc.*, 1969, **91**, 4947.
16. R. G. Pearson, *Accounts Chem. Res.*, 1971, **4**, 152.
17. C. C. Levin, *J. Am. Chem. Soc.*, 1975, **97**, 5649.
18. I. B. Bersuker, *Chem. Rev.*, 2001, **101**, 1067.
19. I. B. Bersuker, *Chem. Rev.*, 2013, **113**, 1351.
20. C.-H. Yang and C.-P. Hsu, *J. Chem. Phys.*, 2013, **139**, 154104.
21. C. Butchosa, S. Simon, L. Blancafort and A. Voityuk, *Phys. Chem. Chem. Phys.*, 2014, **16**, 17154.
22. A. A. Voityuk, *Phys. Chem. Chem. Phys.*, 2012, **14**, 13789.
23. S. Hammes-Schiffer, *Energy & Environmental Science*, 2012, **5**, 7696.
24. R. A. Marcus and N. Sutin, *Biochim. Biophys. Acta*, 1985, **811**, 265.
25. M. K. Johnson, R. B. King, J. Donald M. Kurtz, Charles Kutal, M. L. Norton and R. A. Scott, eds., *Electron Transfer in Biology and the Solid State*, American Chemical Society, Washington DC, 1989.
26. A. A. Kornyshev, M. Tosi and J. Ulstrup, eds., *Electron and Ion Transfer in Condensed Media*, World Scientific, Singapore, 1997.
27. S. Isied, ed., *Electron Transfer Reactions*, American Chemical Society, Washington DC, 1997.
28. A. Kutnetsov and J. Ulstrup, eds., *Electron Transfer in Chemistry and Biology*, Wiley, Hoboken NJ, 1999.
29. V. Balzani, ed., *Electron Transfer in Chemistry. Principles, Theories, Methods and Techniques*, Wiley-VCH, Hoboken NJ, 2001.
30. A. Nitzan, *Annu. Rev. Phys. Chem.*, 2001, **52**, 681.
31. D. M. Guldi, *Chem. Soc. Rev.*, 2002, **31**, 22.
32. T. W. Marin, B. J. Homoelle, K. G. Spears, J. T. Hupp and L. O. Spreer, *J. Phys. Chem. A*, 2002, **106**, 1131.
33. E. A. Plummer and J. I. Zink, *Inorg. Chem.*, 2006, **45**, 6556.
34. S. F. Nelsen, *Adv. Phys. Org. Chem.*, 2006, **41**, 183.
35. V. Coropceanu, J. Cornil, D. A. da Silva Filho, Y. Olivier, R. Silbey and J. L. Brédas, *Chem. Rev.*, 2007, **107**, 926.
36. A. P. Hines, C. M. Dawson, R. H. McKenzie and G. J. Milburn, *Phys. Rev. A*, 2004, **70**, 022303.
37. L. K. McKemmish, R. H. McKenzie, N. S. Hush and J. R. Reimers, *J. Chem. Phys.*, 2011, **135**, 244110/1.
38. Z. Vager, *Chem. Phys. Lett.*, 1997, **273**, 407.
39. J. Trost and K. Hornberger, *Phys. Rev. Lett.*, 2009, **103**, 023202.
40. J. C. Polanyi and A. H. Zewail, *Acc. Chem. Res.*, 1995, **28**, 119.
41. J. Ma, X. Zhu, H. Guo and D. R. Yarkony, *J. Chem. Phys.*, 2012, **137**, 22A541.
42. X. Xu, K. R. Yang and D. G. Truhlar, *J. Chem. Theory Comput.*, 2013, **9**, 3612.
43. X. Zhu and D. R. Yarkony, *J. Chem. Phys.*, 2014, **140**, 024112.
44. J. Dillon and D. R. Yarkony, *J. Phys. Chem. A*, 2013, **117**, 7344.
45. K. R. Yang, X. Xu, J. Zheng and D. G. Truhlar, *Chemical Science*, 2014, **5**, 4661.
46. L. Zhou, B. Jiang, D. Xie and H. Guo, *J. Phys. Chem. A*, 2012, **117**, 6940.
47. C. Xie, J. Ma, X. Zhu, D. H. Zhang, D. R. Yarkony, D. Xie and H. Guo, *J. Phys. Chem. Lett.*, 2014, **5**, 1055.
48. W. Eisfeld, O. Vieuxmaire and A. Viel, *J. Chem. Phys.*, 2014, **140**, 224109.
49. S. Olsen and R. H. McKenzie, *J. Chem. Phys.*, 2012, **136**, 234313/1.
50. T. C. Berkelbach, M. S. Hybertsen and D. R. Reichman, *J. Chem. Phys.*, 2013, **138**, 114102/1.
51. P. Garcia-Fernandez, Y. Liu, I. B. Bersuker and J. E. Boggs, *Phys. Chem. Chem. Phys.*, 2011, **13**, 3502.
52. V. K. Babamov, V. Lopez and R. A. Marcus, *J. Chem. Phys.*, 1983, **78**, 5621.
53. J. Aqvist and A. Warshel, *Chem. Rev.*, 1993, **93**, 2523.
54. D. N. Silverman, *Biochim. Biophys. Acta, Bioenerg.*, 2000, **1458**, 88.
55. A. Warshel, P. K. Sharma, M. Kato, Y. Xiang, H. Liu and M. H. M. Olsson, *Chem. Rev.*, 2006, **106**, 3210.
56. R. A. Marcus, *J. Chem. Phys.*, 2006, **125**, 194504.
57. S. Hammes-Schiffer and A. A. Stuchebrukhov, *Chem. Rev.*, 2010, **110**, 6939.
58. A. Sirjoosingh and S. Hammes-Schiffer, *J. Phys. Chem. A*, 2011, **115**, 2367.
59. A. Sirjoosingh and S. Hammes-Schiffer, *J. Chem. Theory Comput.*, 2011, **7**, 2831.
60. R. H. McKenzie, *Chem. Phys. Lett.*, 2012, **535**, 196.
61. M. S. Baranov, K. A. Lukyanov, A. O. Borissova, J. Shamir, D. Kosenkov, L. V. Slipchenko, L. M. Tolbert, I. V. Yampolsky and K. M. Solntsev, *J. Am. Chem. Soc.*, 2012, **134**, 6025.
62. R. H. McKenzie, *J. Chem. Phys.*, 2014, **141**, 104314/1.
63. P. Politzer, J. R. Reimers, J. S. Murray and A. Toro-Labbe, *J. Phys. Chem. Lett.*, 2010, **1**, 2858.
64. A. Toro-Labbe, *J. Phys. Chem. A*, 1999, **103**, 4398.
65. A. Toro-Labbe, S. Gutierrez-Oliva, J. S. Murray and P. Politzer, *Mol. Phys.*, 2007, **105**, 2619.
66. A. Toro-Labbe, S. Gutierrez-Oliva, J. S. Murray and P. Politzer, *J. Mol. Model.*, 2009, **15**, 707.
67. G. S. Hammond, *J. Am. Chem. Soc.*, 1955, **77**, 334.
68. J. E. Leffler, *Science (Washington, DC, U. S.)*, 1953, **117**, 340.
69. E. Kraka and D. Cremer, *Acc. Chem. Res.*, 2010, **43**, 591.
70. P. Garcia-Fernandez and I. B. Bersuker, *Phys. Rev. Lett.*, 2011, **106**, 246406/1.
71. S. Zilberg, Y. Haas, D. Danovich and S. Shaik, *Angew. Chem., Int. Ed.*, 1998, **37**, 1394.
72. S. Shaik, S. Zilberg and Y. Haas, *Acc. Chem. Res.*, 1996, **29**, 211.
73. S. Shaik, A. Shurki, D. Danovich and P. C. Hiberty, *J. Am. Chem. Soc.*, 1996, **118**, 666.
74. S. Shaik, A. Shurki, D. Danovich and P. C. Hiberty, *Chem. Rev. (Washington, D. C.)*, 2001, **101**, 1501.
75. J. R. Reimers and N. S. Hush, *Chem. Phys.*, 2004, **299**, 79.

76. R. J. Gillespie and R. S. Nyholm, *Quart. Rev. London*, 1957, **11**, 339.
77. R. J. Gillespie and E. A. Robinson, *Angewandte Chemie International Edition in English*, 1996, **35**, 495.
78. R. J. Gillespie, *Coord. Chem. Rev.*, 2000, **197**, 51.
79. R. J. Gillespie, *Coord. Chem. Rev.*, 2008, **252**, 1315.
80. N. V. Sidgwick and H. M. Powell, *Proc. R. Soc. London, Ser. A*, 1940, **176**, 153.
81. J. A. Pople, *Proc. R. Soc. London, Ser. A*, 1950, **202**, 323.
82. R. S. Mulliken, *Rev. Mod. Phys.*, 1942, **14**, 204.
83. A. D. Walsh, *J. Chem. Soc.*, 1953, 2296.
84. A. D. Walsh, *Photoelec. Spectrom. Group Bull.*, 1961, **13**, 348.
85. B. M. Gimarc, *J. Am. Chem. Soc.*, 1971, **93**, 593.
86. K. Mislow and R. D. Baechler, *J. Am. Chem. Soc.*, 1971, **93**, 773.
87. A. H. Pakiari and F. Nazari, *J. Mol. Struct.: THEOCHEM*, 2005, **717**, 189.
88. Y. Arasaki, K. Takatsuka, K. Wang and V. McKoy, *Phys. Rev. Lett.*, 2003, **90**, 248303.
89. R. G. Pearson, *Chem. Phys. Lett.*, 1971, **10**, 31.
90. A. D. Walsh and P. A. Warsop, *Trans. Faraday Soc.*, 1961, **57**, 345.
91. I. B. Bersuker, *Chem. Rev. (Washington, D. C.)*, 2001, **101**, 1067.
92. I. B. Bersuker, *Adv. Quantum Chem.*, 2003, **44**, 1.
93. Y. Liu, I. B. Bersuker, W. Zou and J. E. Boggs, *J. Chem. Theory Comput.*, 2009, **5**, 2679.
94. H. A. Jahn and E. Teller, *Proc. Roy. Soc. A*, 1937, **161**, 220.
95. P. García-Fernández, J. A. Aramburu, M. Moreno, M. Zlatar and M. Gruden-Pavlović, *J. Chem. Theory Comput.*, 2014, **10**, 1824.
96. R. G. Pearson, *Journal of Molecular Structure: THEOCHEM*, 1983, **103**, 25.
97. G. Herzberg and E. Teller, *Z. Phys. Chem.*, 1933, **21**, 410.
98. S. Zilberg and Y. Haas, *J. Phys. Chem. A*, 2011, **115**, 10650.
99. L. Song and J. Gao, *J. Phys. Chem. A*, 2008, **112**, 12925.
100. N. S. Hush, *Z. Elektrochem. Angewandte Physik. Chem.*, 1957, **61**, 734.
101. N. S. Hush, *J. Chem. Phys.*, 1958, **28**, 962.
102. N. S. Hush, *Disc. Farad. Soc.*, 1960, **29**, 113.
103. N. S. Hush, in *Proceedings of the 4th Moscow Conference on Electrochemstry 1956*, English translation: Consultants Bureau, New York, 1961, p. 99.
104. N. S. Hush, *Prog. Inorg. Chem.*, 1967, **8**, 391.
105. C. Creutz and H. Taube, *J. Am. Chem. Soc.*, 1969, **91**, 3988.
106. J. R. Reimers, L. McKemmish, R. H. McKenzie and N. S. Hush, *Phys. Chem. Chem. Phys.*, 2015, **in press, DOI:10.1039/C5CP02237A**.
107. J. R. Reimers, L. McKemmish, R. H. McKenzie and N. S. Hush, *Phys. Chem. Chem. Phys.*, 2015, **in press 10.1039/C5CP02238J**.
108. L. McKemmish, R. H. McKenzie, N. S. Hush and J. R. Reimers, *Phys. Chem. Chem. Phys.*, 2015, **in press DOI:10.1039/C5CP02239H**.
109. J. R. Reimers and N. S. Hush, *J. Phys. Chem.*, 1991, **95**, 9773.
110. J. R. Reimers and N. S. Hush, in *Mixed Valence Systems: Applications in Chemistry, Physics, and Biology*, ed. K. Prassides, Kluwer Acad. Publishers, Dordrecht, 1991, pp. 29.
111. P. Day, N. S. Hush and R. J. H. Clark, *Phil. Trans. Roy. Soc. A*, 2008, **366**, 5.
112. N. S. Hush, *J. Electroanal. Chem.*, 1999, **460**, 5.
113. S. B. Piepho, E. R. Krausz and P. N. Schatz, *J. Am. Chem. Soc.*, 1978, **100**, 2996.
114. R. A. Marcus and N. Sutin, *Biochim. Biophys. Acta*, 1985, **811**, 265.
115. N. S. Hush, *ACS Symp. Ser.*, 1982, **198**, 301.
116. J. R. Reimers, B. B. Wallace and N. S. Hush, *Phil. Trans. Roy. Soc. A*, 2008, **366**, 15.
117. K. D. Demadis, C. M. Hartshorn and T. J. Meyer, *Chem. Rev.*, 2001, **101**, 2655.
118. E. B. D. Wilson, J. C; Cross, Paul C., *Molecular Vibrations: The Theory of Infrared and Raman Vibrational Spectra*, McGraw-Hill Book Company, New York, 1955.
119. N. S. Hush, *Chem. Phys.*, 1975, **10**, 361.
120. G. Fischer, *Vibronic Coupling*, Academic Press, London, 1984.
121. J. R. Reimers and N. S. Hush, *J. Am. Chem. Soc.*, 2004, **126**, 4132.
122. R. J. Cave and M. D. Newton, *Chem. Phys. Lett.*, 1996, **249**, 15.
123. J. R. Reimers, W. A. Shapley, A. P. Rendell and N. S. Hush, *J. Chem. Phys.*, 2003, **119**, 3249.
124. D. S. Talaga and J. I. Zink, *J. Phys. Chem. A*, 2001, **105**, 10511.
125. J. V. Lockard, J. I. Zink, A. E. Konradsson, M. N. Weaver and S. F. Nelsen, *J. Am. Chem. Soc.*, 2003, **125**, 13471.
126. R. Kubo and Y. Toyozawa, *Prog. Theor. Phys.*, 1955, **13**, 160.
127. O. Kanchanawong, M. G. Dahlbom, T. P. Treynor, J. R. Reimers, N. S. Hush and S. G. Boxer, *J. Phys. Chem. B*, 2006, **110**, 18688.
128. J. Swalen and J. Ibers, *J. Chem. Phys.*, 1962, **36**, 1914.
129. S.-H. Lee, A. G. Larsen, K. Ohkubo, Z.-L. Cai, J. R. Reimers, S. Fukuzumi and M. J. Crossley, *Chem. Sci.*, 2011, **3**, 257.
130. S. N. Yurchenko, R. J. Barber, J. Tennyson, W. Thiel and P. Jensen, *J. Mol. Spectrosc.*, 2011, **268**, 123.
131. X. Huang, D. W. Schwenke and T. J. Lee, *J. Chem. Phys.*, 2011, **134**, 044320.
132. J. Pesonen, A. Miani and L. Halonen, *J. Chem. Phys.*. 2001, **115**, 1243.
133. R. G. A. R. Maclagan, *Mol. Phys.*, 1980, **41**, 1471.
134. H. J. Werner and P. J. Knowles, *J. Chem. Phys.*, 1985, **82**, 5053.
135. P. J. Knowles and H. J. Werner, *Chem. Phys. Letts.*, 1985, **115**, 259.
136. D. Hegarty and M. A. Robb, *Molec. Phys.*, 1979, **38**, 1795.
137. I. B. Bersuker, N. N. Gorinchoi and V. Z. Polinger, *Theor. Chim. Acta*, 1984, **66**, 161.
138. N. V. Cohan and C. A. Coulson, *Trans. Faraday Soc.*, 1956, **52**, 1163.
139. J. P. Foster and F. Weinhold, *J. Am. Chem. Soc.*, 1980, **102**, 7211.
140. W. J. Hehre, R. F. Stewart and J. A. Pople, *J. Chem. Phys.*, 1969, **51**, 2657.
141. C. Møller and M. S. Plesset, *Phys. Rev. A*, 1934, **46**, 618.
142. H.-J. Werner, P. J. Knowles, F. R. Manby, M. Schütz, P. Celani, G. Knizia, T. Korona, R. Lindh, A. Mitrushenkov, G. Rauhut, T. B. Adler, R. D. Amos, A. Bernhardsson, A. Berning, D. L. Cooper, M. J. O. Deegan, A. J. Dobbyn, F. Eckert, E. Goll, C. Hampel, A. Hesselmann, G. Hetzer, T. Hrenar, G. Jansen, C. Köppl, Y. Liu, A. W. Lloyd, R. A. Mata, A. J. May, S. J. McNicholas, W. Meyer, M. E. Mura, A. Nicklass, P. Palmieri, K. Pflüger, R. Pitzer, M. Reiher, T. Shiozaki, H. Stoll, A. J. Stone, R. Tarroni, T. Thorsteinsson, M. Wang and A. Wolf, *MOLPRO, version 2010.1, a package of ab initio programs*, University of Birmingham, Birmingham, 2010.
143. X. Zhang and J. M. Herbert, *J. Chem. Phys.*, 2015, **142**, 064109.
144. X. Zhang and J. M. Herbert, *J. Chem. Phys.*, 2014, **141**, 064104.
145. A. Migliore, N. F. Polizzi, M. J. Therien and D. N. Beratan, *Chem. Rev.*, 2014, **114**, 3381.
146. Y. Yang and O. Kühn, *Chem. Phys. Lett.*, 2011, **505**, 1.
147. V. Zoete and M. Meuwly, *J. Chem. Phys.*, 2004, **120**, 7085.
148. T. Asada, H. Haraguchi and K. Kitaura, *J. Phys. Chem. A*, 2001, **105**, 7423.
149. P. Garcia-Fernandez, L. Garcia-Canales, J. M. Garcia-Lastra, J. Junquera, M. Moreno and J. A. Aramburu, *J. Chem. Phys.*, 2008, **129**, 124313/1.
150. Y. K. Yang, O., G. Santambrogio, D. J. Goebbert and K. R. Asmis, *J. Chem. Phys.*, 2008, **129**, 224302.
151. Y. Wang and J. R. Gunn, *Int. J. Quantum Chem.*, 1999, **73**, 357.
152. R. H. McKenzie, C. Bekker, B. Athokpam and S. G. Ramesh, *J. Chem. Phys.*, 2014, **140**, 174508/1.

153. R. A. Kendall, T. H. Dunning, Jr. and R. J. Harrison, *J. Chem. Phys.*, 1992, **96**, 6796.
154. Y. Horbatenko and S. F. Vyboishchikov, *ChemPhysChem*, 2011, **12**, 1118.
155. D. M. Friedrich and W. M. McClain, *Chem. Phys. Lett.*, 1975, **32**, 541.
156. N. Mikami and M. Ito, *J. Chem. Phys.*, 1976, **64**, 3077.
157. R. P. Rava, L. Goodman and K. Krogh-Jespersen, *J. Chem. Phys.*, 1981, **74**, 273.
158. N. Mikami and M. Ito, *Chem. Phys.*, 1977, **23**, 141.
159. L. Blancafort and M. Sola, *J. Phys. Chem. A*, 2006, **110**, 11219.
160. A. G. Ozkabak, L. Goodman and K. B. Wiberg, *J. Chem. Phys.*, 1990, **92**, 4115.
161. J. Murakami, K. Kaya and M. Ito, *J. Chem. Phys.*, 1980, **72**, 3263.
162. R. Berry, *J. Chem. Phys.*, 1961, **35**, 2253.
163. C. Angeli, R. Cimiraglia, S. Evangelisti, T. Leininger and J. P. Malrieu, *J. Chem. Phys.*, 2001, **114**, 10252.
164. J. R. Reimers, G. B. Bacskay and S. Nordholm, *J. Chem. Educ.: Software*, 1998, **10B**, 1.
165. G. B. Bacskay, J. R. Reimers and S. Nordholm, *J. Chem. Educ.*, 1997, **74**, 1494.
166. G. B. Bacskay and S. Nordholm, *J. Phys. Chem. A*, 2013, **117**, 7946.

Cite this: DOI: 10.1039/c0xx00000x

www.rsc.org/xxxxxx

ARTICLE TYPE

TOC graphic

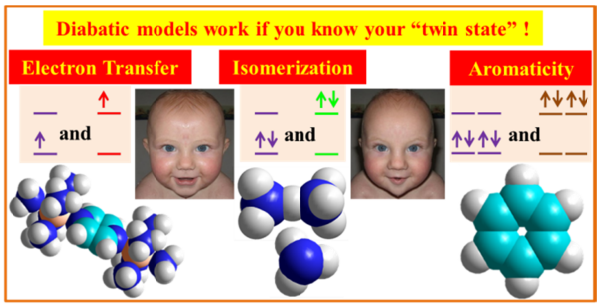

NOVELTY STATEMENT: A way is found for describing general chemical reactions using diabatic multi-state and "twin-state" models.